Nano Research

ISSN 1998-0124 CN 11-5974/O4
https://doi.org/10.1007/s12274-023-5660-8

Review Article

Recent advances in high-performance triboelectric nanogenerators

Di Liu[1,2,§], Yikui Gao[1,2,§], Linglin Zhou[1,2], Jie Wang[1,2] (✉), and Zhong Lin Wang[1,2,3] (✉)

[1] *Beijing Institute of Nanoenergy and Nanosystems, Chinese Academy of Sciences, Beijing 101400, China*
[2] *College of Nanoscience and Technology, University of Chinese Academy of Sciences, Beijing 100049, China*
[3] *School of Materials Science and Engineering, Georgia Institute of Technology, Atlanta, GA 30332, USA*
[§] *Di Liu and Yikui Gao contributed equally to this work.*

Received: 29 January 2023 / **Revised:** 14 February 2023 / **Accepted:** 9 March 2023

ABSTRACT

The development of the Internet of Things (IoT) and artificial intelligence has accompanied the evolution of energy demand and structure in the new era, and the power sources for billions of distributed electronics and sensors have aroused worldwide interest. As an alternative energy harvesting technology, triboelectric nanogenerators (TENGs) have received remarkable attention and have shown attractive potential applications for use in micro/nano power sources, self-powered sensors, high-voltage power sources, and blue energy due to their advantages of small size, light weight, flexibility, low cost, and high efficiency at low frequency. In this review, we discuss high-performance TENGs from the perspectives of triboelectric charge density, output voltage, energy density, and corresponding quantification methods. Among these topics, the limitations, optimization methods and techniques, and potential directions to challenge these limits are comprehensively discussed and reviewed. Finally, we discuss the emerging challenges, strategies, and opportunities for research and development of high-performance TENGs.

KEYWORDS

high-performance triboelectric nanogenerator (TENG), charge density, voltage, energy density, average power density

1 Introduction

The massive utilization of fossil fuels over the last century inevitably brings the problems of global warming, environmental pollution, energy crisis, and an increase in the disordered, low-quality, and high-entropy energy distributed around the environment. These important and urgent energy issues have promoted researchers to find green energy sources and develop new energy harvesting technologies [1]. Particularly, entering the new era of artificial intelligence and Internet of Things (IoT) possessing billions of distributed sensors, it is very challenging to power these enormous, widely distributed, and low-power electronics relying only on conventional methods such as batteries, supercapacitors, and solar cells. With the merits of wide material choice, simple structure, easy fabrication, low cost, light weight, flexibility, and high efficiency even at low frequency, triboelectric nanogenerators (TENGs) show great potential and are considered a revolutionary energy harvesting technology for low-amplitude, low-quality, and high-entropy energy [2, 3]. To date, TENGs have displayed broad applications as micro/nano power sources [4–8], self-powered sensors [9–12], blue energy sources [13–16], and new high-voltage power sources [17–19], covering the areas of environmental science [20–24], implantable/wearable electronics [25–27], human–machine interfaces [28–30], smart cities [31], intelligent agriculture [32, 33], security [34], and so on. They have aroused worldwide interest among 80 countries, and more than 10,000 scientists have worked in this research field since the invention of TENGs in 2012, which has also stimulated the rapid development of this research field [35].

As an energy harvester, TENGs can convert mechanical energy into electricity based on the conjunction of triboelectrification and electrostatic induction. In the last ten years, great efforts have been devoted to studying the fundamental working mechanism of TENGs and elevating their output performance, further advancing their broad impact on energy and sensors. To date, the peak power density and average power density of TENGs have reached 10 $MW \cdot m^{-2}$ [36] and 87.26 $W \cdot m^{-2} \cdot Hz^{-1}$ [37], respectively, and an energy conversion efficiency higher than 50% can also be achieved in some special conditions [37, 38], which is also comparable with the output power of the solar cell. In addition, with the merits of high impedance, high voltage, and controlled output charges, TENGs can easily produce several kV to dozens of kV output voltages, offering great potential as new high voltage power sources for highly sensitive nanocoulomb molecular mass spectrometry [39], plasma generation [40], negative air ion generation for air purification [41], facilitating plant growth [33], droplet manipulation [42], and actuators [43].

The rapid development of high-performance TENGs has greatly promoted this research field and attracted more researchers to devote themselves to the research of micro/nano energy, which formed a virtuous circle. In the past few years, many reviews have focused on the theoretical modelling, energy harvesting, self-powered sensors of TENGs, and the representative applications of TENGs in specific fields. Here, we provide a bird's eye view of high-performance TENGs with a focus on three representative and standard electric parameters, including triboelectric charge density (TECD) [44–51], output voltage

Address correspondence to Jie Wang, wangjie@binn.cas.cn; Zhong Lin Wang, zhong.wang@mse.gatech.edu

[52–54], and energy density (average power density) [36, 37, 55, 56] (Fig. 1). We hope the knowledge and insights in this timely review will provide valuable information for the wide science community in three aspects: (1) understanding the key limitations to realizing high-performance TENGs; (2) stimulating the development of advanced technologies for high-performance TENGs; and (3) encouraging the establishment of performance evaluation and test standards. This review begins with the basic principle of TENGs with a highlight on standards for quantifying the performance of TENGs and then elaborates on high-performance TENGs from the perspectives of triboelectric charge density, output voltage, energy density, and corresponding quantification methods. Among these topics, the limitations, optimization methods and techniques, and potential directions to challenge these limits are comprehensively discussed and reviewed. We then conclude with a summary of the emerging challenges, strategies, and opportunities for the research and development of high-performance TENGs.

2 Basic principle of TENGs

TENGs convert mechanical energy into electricity through contact electrification (CE) and electrostatic induction effects. In this section, we will discuss the origin of contact electrification, the fundamental physics and basic working modes of TENGs, and the standards for quantifying the performance of TENGs.

2.1 Origin of contact electrification

Contact electrification (or triboelectrification), which refers to the charge transfer between two identical or different materials, is an old physical phenomenon dating back to ancient times and commonly exists in nature and our daily life [57]. In the last long time, it has generally been considered a negative phenomenon because electrostatic charges often cause electrostatic discharge (ESD) failure of electronic components and integrated circuits (ICs), ignite deadly dust explosions, disrupt flow, and lead to increased friction and energy losses [58], so it is only successfully used in limited useful technologies such as photocopying, laser printing, electrostatic self-assembly, and TENGs. Specifically, the invention and fast development of TENGs also stimulate fundamental research on contact electrification. Moreover, it also draws broad interest across different scientific communities, especially the fundamental research of triboelectrification, to establish the scientific basis of this new energy technology and largely improve its performance.

By using Kelvin probe force microscopy (KPFM) to study the fundamental mechanism of CE, the conclusion that electron transfer is the dominant mechanism of CE between solid–solid pairs is obtained [59–62]. The triboelectrification effect is the interfacial charge transfer phenomenon when two materials come into contact with each other. However, the critical issues are how close the two atoms are and how electrons will transfer from one atom to the other, which are answered by amplitude modulation-atomic force microscopy (AM-AFM). The probe cantilever was excited near its resonance frequency (f_0), with the free vibration amplitude (A_0) setting before the tip engaged the surface of the sample and the set-point vibration amplitude (A_{sp}) setting as a feedback parameter to measure the topography of the sample surface after engagement. A typical measurement process with two passes in one scan line is adopted. The first pass is a topography scan by using the tip to tap the sample, and the second pass is a potential difference (ΔV) measurement between the tip

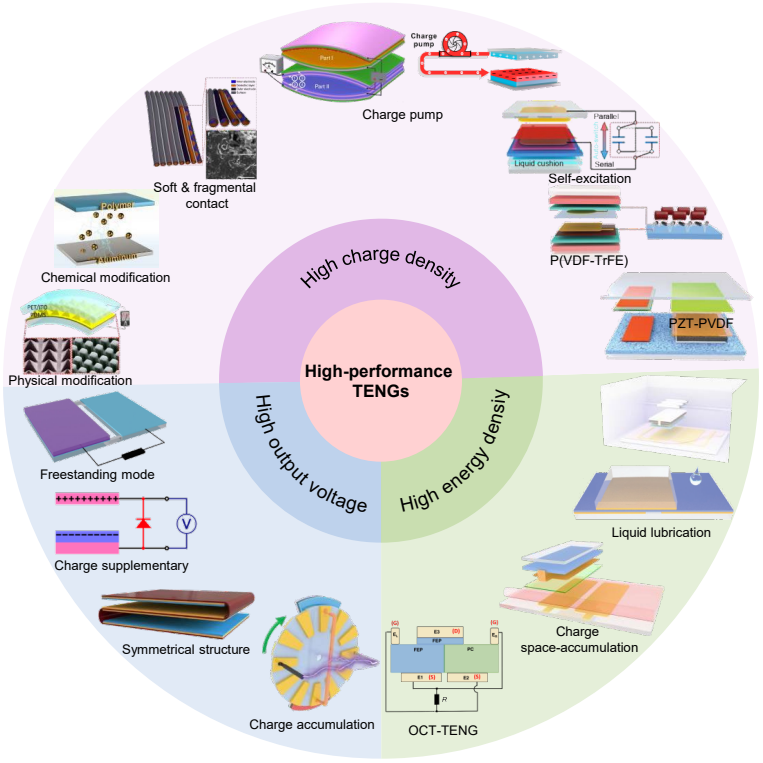

Figure 1 An overview diagram of high-performance TENGs. Reproduced with permission from Ref. [44], © American Chemical Society 2012. Reproduced with permission from Ref. [46], © Elsevier Ltd. 2018. Reproduced with permission from Ref. [47], © WILEY-VCH Verlag GmbH & Co. KGaA, Weinheim 2020. Reproduced with permission from Ref. [48], © Cheng, L. et al. 2018. Reproduced with permission from Ref. [49], © Wang, J. et al. 2016. Reproduced with permission from Ref. [50], © Liu, W. L. et al. 2019. Reproduced with permission from Ref. [51], © Wiley-VCH GmbH 2022. Reproduced with permission from Ref. [52], © WILEY-VCH Verlag GmbH & Co. KGaA, Weinheim 2014. Reproduced with permission from Ref. [53], © American Chemical Society 2018. Reproduced with permission from Ref. [54], © The Royal Society of Chemistry 2020. Reproduced with permission from Ref. [36], © Wu, H. et al. 2021. Reproduced with permission from Ref. [55], © He, W. C. et al. 2020. Reproduced with permission from Ref. [56], © Wiley-VCH GmbH 2020. Reproduced with permission from Ref. [37], © He, W. C. et al. 2022.

and the sample. The basic principle is that the phase shift will be 90° if there is no interaction force between the probe and the sample; the phase shift ($\Delta\varphi$) will increase ($\Delta\varphi > 0$) if the interaction force is a net attractive force; and the phase shift will decrease ($\Delta\varphi < 0$) if the interaction force is a net repulsive force. In other words, the interaction force between the tip and sample will change the vibration phase shift.

Based on the above theory, Li et al. studied the relationships of ΔV–A_{sp} and $\Delta\varphi$–A_{sp} to explore the relevance between the change in the vibration phase shift and CE in tapping mode [59]. In this experiment, there are three different A_0 values (100, 70, and 50 nm) with various A_{sp} values for each A_0 (Figs. 2(a)–2(f)). In the case of A_0 = 50 nm, ΔV is approximately 0, and $\Delta\varphi < 0$ is not observed with increasing A_{sp}. By increasing the free vibration amplitudes (A_0 = 70 and 100 nm), which means that the probe cantilever can vibrate with more energy and the tip of the probe will approach the surface of the sample, there is a dramatic increase in ΔV from 0, and the interaction force region is changed from the attractive regime to the repulsive force regime with increasing A_{sp} (Fig. 2(g)). In other words, the distance of two atoms for electron transfer should be smaller than the interatomic distance at equilibrium. This was followed in 2020 by studying the temperature and bias effects on the CE, and the electron transfer between the tip and the samples still occurs only when the tip works in the repulsive force region [63].

This can be easily understood by the interatomic interaction

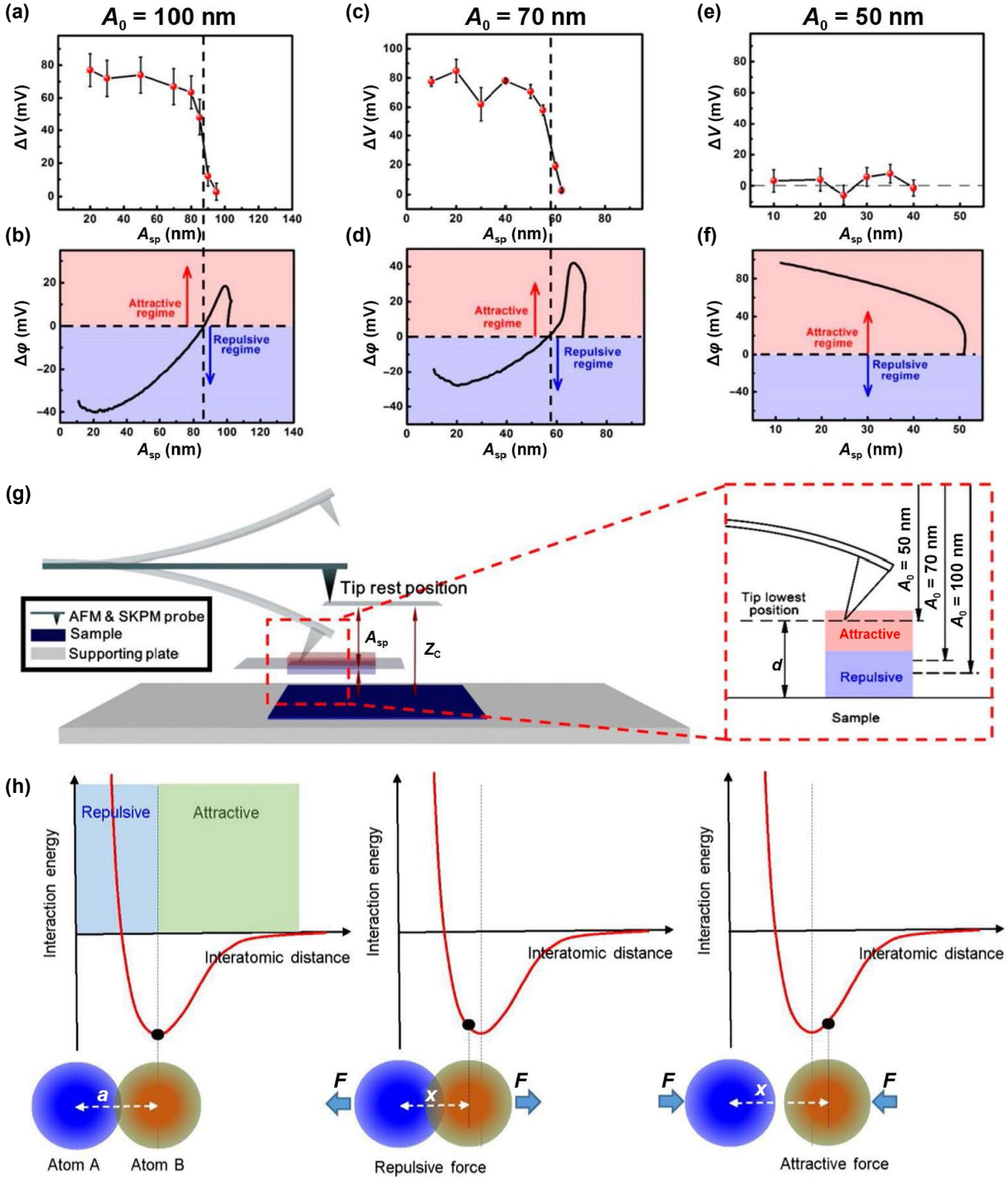

Figure 2 Origin of contact electrification. (a)–(f) The relationships between ΔV–A_{sp} and $\Delta\varphi$–A_{sp} at A_0 = 100, 70, and 50 nm. (g) The schematic diagram shows the relationship between the vibration distance and the interaction force region. Reproduced with permission from Ref. [59], © American Chemical Society 2016. (h) The schematic diagrams show the interaction energy and the interatomic distance between two atoms. Reproduced with permission from Ref. [57], © Elsevier Ltd. 2019.

potential (Fig. 2(h)) [57]. Two atoms form a bond, establishing an equilibrium state with an equilibrium distance (a), and there is partial overlap in electronic clouds or wave functions. In the CE process, an external force is applied to let the two surfaces come into contact, and the interatomic distance (x) is forced to be shorter than a between the contacting points at atomic and nanoscales, establishing the local repulsive force owing to the increased overlap of electronic clouds. The strong overlap of electronic clouds permits electron transfer. If x is larger than a, the two atoms tend to attract each other owing to the reduced overlap of electronic clouds, which may break their bond. Overall, the mechanical force plays the role of causing a strong overlap of electron clouds of two atoms as much as possible, leading to charge transfer in the repulsive region.

2.2 Four working modes of the TENG

The basic working modes of TENGs can be divided into four modes (Fig. 3(a)): contact–separation (CS) mode, lateral sliding (LS) mode, single electrode (SE) mode, and freestanding triboelectric-layer (FT) mode. In addition, according to the mode of friction, they can be classified as contact mode and sliding mode TENGs; and according to the number of dielectric layers, they can also be divided into single dielectric-layer and double dielectric-layer TENGs. Due to the different structures and electrode arrangements, the four working modes of TENGs have different application scenarios.

The CS-TENG utilizes the vertical movement of the charged triboelectric layer to drive induced electrons flowing in an external circuit, which has the advantages of a simple structure, small material wear, and easy application in practice, so it is the most widely used mode in vibration energy harvesting [64], self-powered sensors [65], implantable and wearable power sources [66], and blue energy [14]. The LS-TENG can convert the mechanical energy in the horizontal direction to electricity, which

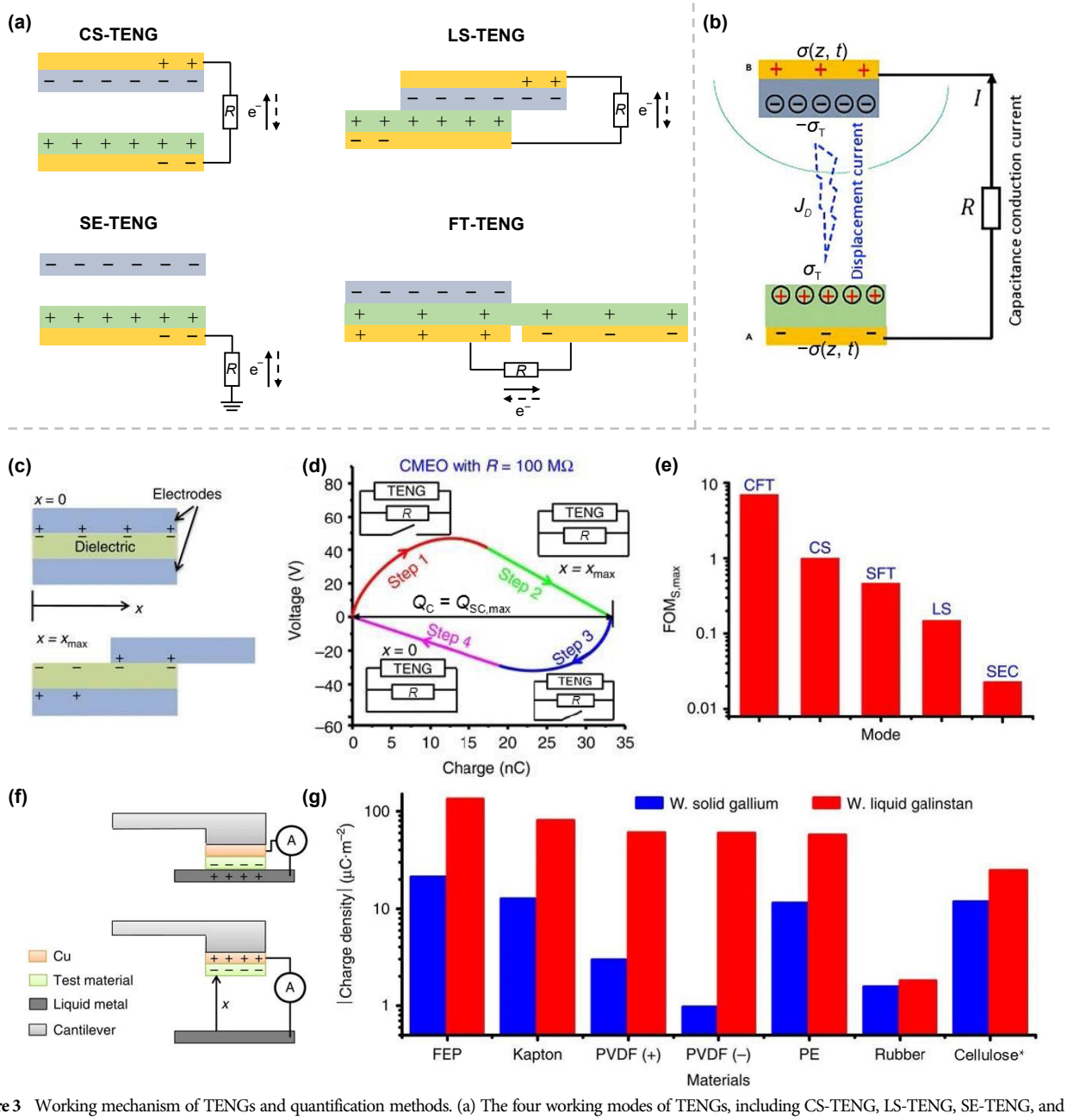

Figure 3 Working mechanism of TENGs and quantification methods. (a) The four working modes of TENGs, including CS-TENG, LS-TENG, SE-TENG, and FT-TENG. (b) The working mechanism of the TENG. Reproduced with permission from Ref. [76], © Elsevier Ltd. 2019. (c) The schematic diagram shows the LS-TENG. (d) The voltage–charge cycle of the LS-TENG at a load of 100 MΩ combined with a switch in parallel. (e) The maximum FOM_S of the CFT, CS, SFT, LS, and SEC mode TENGs. (f) The measurement equipment for testing the surface charge density of various dielectric materials with the liquid metal as one electrode. (g) The surface charge density of various dielectric materials with the liquid metal as one electrode. Reproduced with permission from Ref. [77], © Zi, Y. L. et al. 2015.

can work in rotary motion and realize a stable output charge and current for applications such as sensitive nanocoulomb molecular mass spectrometry [39] as well as microfluidic transport systems [67]. The SE-TENG is invented to harvest the mechanical energy of a free object without attaching an electric connection, which shows significant merits for harvesting energy in some special cases, such as human working [68], finger typing [69], motion sensors [70], and raindrops [71]. In addition, the FT-TENG is also invented for harvesting mechanical energy from a free object [72], and it is well suited for rotary motion energy harvesting. A distance can exist between the dielectric layer and the electrode, which is beneficial for extending the durability and decreasing the material wear of sliding TENGs. This mode has been widely used for electrochemistry, energy storage, environmental mechanical energy harvesting, angle sensors, and high-voltage power sources [20, 41, 73]. The theoretical model and detailed working mechanism of these four modes of TENGs have been extensively reviewed in many previous works and thus are not covered in detail here. Based on these four basic working modes, various TENG structures are designed for practical applications depending on the working environment and requirements.

2.3 Maxwell's displacement current

Generally, the physical model of a TENG can be referred to as a capacitive model, which consists of a voltage source and a variable capacitor. The external force applied on the TENG alters the variable capacitance. The capacitance between the two electrodes varies with the repeated change in separating distance (corresponding to the contact–separation type TENG) and contact area (corresponding to the sliding type TENG), resulting in charges flowing back and forth in the external circuit with an alternating current produced. This qualitative capacitive model is very useful to intuitively understand the working mechanism of TENGs and guide TENG structure design as well as performance optimization, combining with Ohm's law. Furthermore, three-dimensional spatial models using the displacement-dependent electric field concept based on Maxwell's equations are proposed to better understand the practical output behavior of TENGs on external loads [74, 75].

With a deep understanding of the fundamental physics of TENGs, especially the introduction of a polarization term P_s (representing the polarization owing to the preexisting electrostatic charges on the media, arising from the surface electrostatic charges) in the displacement vector by professor Wang [76], it is revealed that the displacement current is the fundamental basis of TENGs, from which the output performance of TENGs can be calculated. The displacement current density (J_D) is defined as

$$J_D = \frac{\partial D}{\partial t} = \varepsilon \frac{\partial E}{\partial t} + \frac{\partial P_s}{\partial t} \tag{1}$$

where D is the displacement field, t represents time, ε is the medium permittivity, and E is the electric field, respectively. The first term represents a time-varying electric field, giving birth to electromagnetic wave theory; and the second term presents the nonelectric field-induced polarization in the displacement from surface polarization, setting the foundation for the TENG (Fig. 3(b)).

By integrating the displacement current density on the surface, the displacement current (I_D) can be obtained by Eq. (2)

$$I_D = \int J_D \cdot \mathrm{d}S = \int \frac{\partial D}{t} \cdot \mathrm{d}S = \frac{\partial}{\partial t} \int \nabla \cdot D \mathrm{d}r = \frac{\partial}{\partial t} \int \rho \mathrm{d}r = \frac{\partial Q}{\partial t} \tag{2}$$

where S is the medium surface, r is the field point, ρ is the distribution of free charges, and Q is the total free charges on the electrode, respectively. It is noted that the displacement current is the intrinsic physical core of current generation representing the internal driving force, and the observed capacitive conduction current in the external circuit is the external manifestation of displacement current, which forms a complete loop at the two metal electrodes. Based on this theory, the output power of TENGs can be calculated and optimized by reasonable structural design of the dielectric layer, the electrode layer, and the integrated device, which is very useful for guiding the design of highly efficient TENGs [76].

2.4 Methods for quantifying the performance of TENGs

As an energy harvester, the standardized methods and parameters for quantifying the performance of different TENGs with varying structures and materials are very important for guiding the design of different requirements of TENGs in practical applications, facilitating communication between different research groups, promoting the industrialization of TENGs, and stimulating the benign development of this research field. The figure-of-merits (FOMs) for TENGs were first proposed in 2015 based on the operation energy output cycle of the built-up voltage (V) against the transferred charge (Q) [77]. The enclosed area of the V–Q plot represents the output energy of the TENG. It is noted that the largest encircled area has the maximum possible output energy (E_m, denoted as cycles for maximized energy output (CMEO)), which corresponds to the maximum open-circuit voltage ($V_{OC,max}$), the maximum short-circuit transferred charge ($Q_{SC,max}$), and the maximum achievable absolute voltage (V'_{max}) at $Q = Q_{SC,max}$, as described by Eq. (3)

$$E_m = \frac{1}{2} Q_{SC,max} \left(V_{OC,max} + V'_{max} \right) \tag{3}$$

This E_m can be considered the maximum theoretical possible output energy per cycle of the TENG at any working mode. To exclude the effect of structure and motion parameters on the output energy, a dimensionless structural FOM (FOM_S) can be derived as

$$FOM_S = \frac{2\varepsilon_0}{\sigma^2} \frac{E_m}{A x_{max}} \tag{4}$$

where ε_0 is the vacuum permittivity, σ^2 can be considered the material FOM (FOM_M), A is the effective electrostatic induction area, and x_{max} is the maximum displacement of two triboelectric layers, respectively. Thus, the performance FOM (FOM_P) can be defined as

$$FOM_P = FOM_S \cdot \sigma^2 = 2\varepsilon_0 \frac{E_m}{A x_{max}} \tag{5}$$

Based on the above FOMs, the performance of various TENGs can be evaluated and compared.

A simple method is also presented to realize the maximum possible cycle of energy output relying on a mechanical switch triggered by the motion of the TENG to instantaneously discharge the TENG at the maximum and minimum displacements, which is operated at CMEO (Figs. 3(c) and 3(d)). With the help of the finite element method (FEM), the FOMs of TENGs with different working modes can be simulated as contact FT (CFT) > CS > sliding FT (SFT) > LS > SE contact (SEC) (Fig. 3(e)). It is found that the FOM_S of the CFT mode TENG is the highest, which benefits from the dramatically decreased capacitance between the two electrodes and the enhanced induction charges by the double-sided triboelectrification of the middle layer. This was followed in 2019 by considering the air breakdown effect, and the updated FOMs were given [78]. Furthermore, a representative matrix for measuring the triboelectric performance of materials is also

presented with the liquid metal as the counterpart material in a controlled environment (Fig. 3(f)). The low contact intimacy caused by surface roughness in solid materials can be greatly increased, and a simple quantified triboelectric order is obtained (fluorinated ethylene propylene (FEP)–Kapton–polyvinylidene fluoride (PVDF)–polyethylene (PE)–nature rubber–galinstan –cellulose, from negative to positive polarity) (Fig. 3(g)), setting the foundation for quantifying the performance of different materials.

3 Improving charge density

TECD dominates the output capability of TENGs, such as output charges, current, voltage, and power. Specifically, the output power density has a quadratic relationship with the TECD, so great efforts are devoted to improving the TECD, and then the output power can be greatly elevated.

3.1 Limitations of charge density

The maximum surface charge density of the TENG (σ_{max}) can be described as [79]

$$\sigma_{max} = (\sigma_{triboelectrification}, \sigma_{air\ breakdown}, \sigma_{dielectric\ breakdown})\ \min \quad (6)$$

where $\sigma_{triboelectrification}$ represents the triboelectric charge density, $\sigma_{air\ breakdown}$ is the maximum surface charge density limited by the air breakdown effect, and $\sigma_{dielectric\ breakdown}$ is the maximum surface charge density restricted by the dielectric breakdown effect, respectively. Electrostatic breakdown is a very common phenomenon in our daily life, such as lightning and the discharge of a finger touching the doorknob, because of the inherent high voltage characteristics of electrostatic charges. It is also a common phenomenon widely existing in any working mode of TENGs, and $\sigma_{air\ breakdown}$ is often the smallest value in TENGs. In 2014, Wang et al. first demonstrated that the air breakdown between two triboelectric layers restricts the maximum surface charge density in the CS-TENG by employing the corona discharge technique (Fig. 4(a)) [80]. Paschen's law was first introduced into the governing equation of the CS-TENG to understand σ_{max} and the maximized output performance of the CS-TENG. Generally, the gap voltage across the air gap of the CS-TENG should be smaller than the breakdown voltage determined by Paschen's law over the whole working distance of the CS-TENG (Fig. 4(b)). The maximum surface charge density restricted by air breakdown under short-circuit conditions ($\sigma_{max,SC}$) can be described as

$$\sigma_{max,SC} = \left\{ \frac{AP\varepsilon_0 (t + d\varepsilon_r)}{[\ln(Pd + B)]\, t} \right\} \min \quad (7)$$

where A and B are gas constants, and P, ε_0, d, ε_r, and t are the atmospheric pressure, vacuum permittivity ($\varepsilon_0 \approx 8.85 \times 10^{-12}$ F·m^{-1}), gap distance, relative permittivity, and thickness of the dielectric layer, respectively. In addition, under open-circuit conditions, the electrons cannot be transferred in a timely manner between the two electrodes [81, 82], and the σ_{max} restricted by air breakdown under open-circuit conditions ($\sigma_{max,OC}$) can be described as

$$\sigma_{max,OC} = \left\{ \frac{AP\varepsilon_0}{\ln(Pd) + B} \right\} \min \quad (8)$$

It is noted that $\sigma_{max,OC}$ is only ~ 50 μC·m^{-2} for a general TENG with a moving displacement from 0 to 0.01 m. $\sigma_{dielectric\ breakdown}$ can be understood by Gauss's theorem, and the maximum electric field applied on the dielectric layer is described as

$$\sigma_{dielectric\ breakdown} = \varepsilon_0 \varepsilon_r E_b \quad (9)$$

where E_b represents the critical breakdown field strength of the dielectric layer.

Based on the above theory, the output performance of the CS-TENG can be improved by optimizing the parameters in Eq. (7). A high vacuum environment was applied to avoid air breakdown, and a high output charge density of 1003 μC·m^{-2} was realized with the $BaTiO_3$ ferroelectric material (Fig. 4(c)) [79]. By regulating the atmosphere pressure and the gas components (P, A, and B in Eq. (7)), air breakdown can be restrained, and the output charge density of the CS-TENG can also be improved (Fig. 4(d)) [82]. Reducing the thickness and increasing the relative permittivity of the dielectric layer (t and ε_r in Eq. (7)) are simple and effective methods to improve the output charge density of the CS-TENG under atmospheric conditions (Figs. 4(e) and 4(f)) [83]. These works also demonstrate the limiting factors of charge density in CS-TENGs.

Different from the CS-TENG, the breakdown effect in the sliding mode TENG is very complex. For instance, as the unique structure of sliding FT-TENGs, there are two breakdown types that could occur, including breakdown between two electrodes and breakdown across the dielectric layer (Fig. 4(g)). Both the simulated results by COMSOL software and the experimental results demonstrate the two types of breakdown in the sliding FT-TENG (Fig. 4(h)) [84]. It is noted that these breakdown types are closely related to the distance between two electrodes and the material's type of moving part (metal or dielectric material). A large distance between two electrodes is very beneficial to avoiding the first breakdown type, and the second breakdown type can be largely prevented when the moving part is a dielectric. It should be stressed that these breakdown types easily occur with a large external load or in open-circuit conditions. Recently, a more common and usually ignored breakdown type between the sliding surface has been demonstrated, which greatly limits the maximum surface charge density of the dielectric layer (Fig. 4(i)) [56]. The output charges at various atmosphere pressures imply that the possible breakdown distance is at approximately the micrometer level (Fig. 4(j)), which is equivalent to the surface roughness. If air breakdown in the triboelectric surface is avoided with the specially chosen oil filling this gap [56] or adding an upper shielding electrode [55], the output charge density of the sliding mode TENG will be improved remarkably.

3.2 Improving surface charge density

Improving the surface charge density is the most straightforward and effective direction to enhance the output performance of TENGs, which mainly includes material optimization, structural design, environmental control, ultrathin dielectric layers, and liquid lubrication.

3.2.1 Material optimization

Material optimization can be understood by three aspects: material choice, surface physical modification, and surface chemical modification. Material choice is widely used to choose suitable triboelectric materials for improving the performance of TENGs and other electrostatic applications, and this often relies on the triboelectric series. The triboelectric series, which is obtained only by mutually rubbering two materials, is an ordering of materials such that one material tending to lose electrons is placed in the positive end, while the material tending to gain electrons is placed in the negative end. Obviously, the conventional triboelectric series is empirical, and only the charge polarity is considered. In 2019, a representative quantified triboelectric series was proposed based on a controlled platform and environment, and both the charge polarity and quantity were considered in this series, providing a guideline for material choice

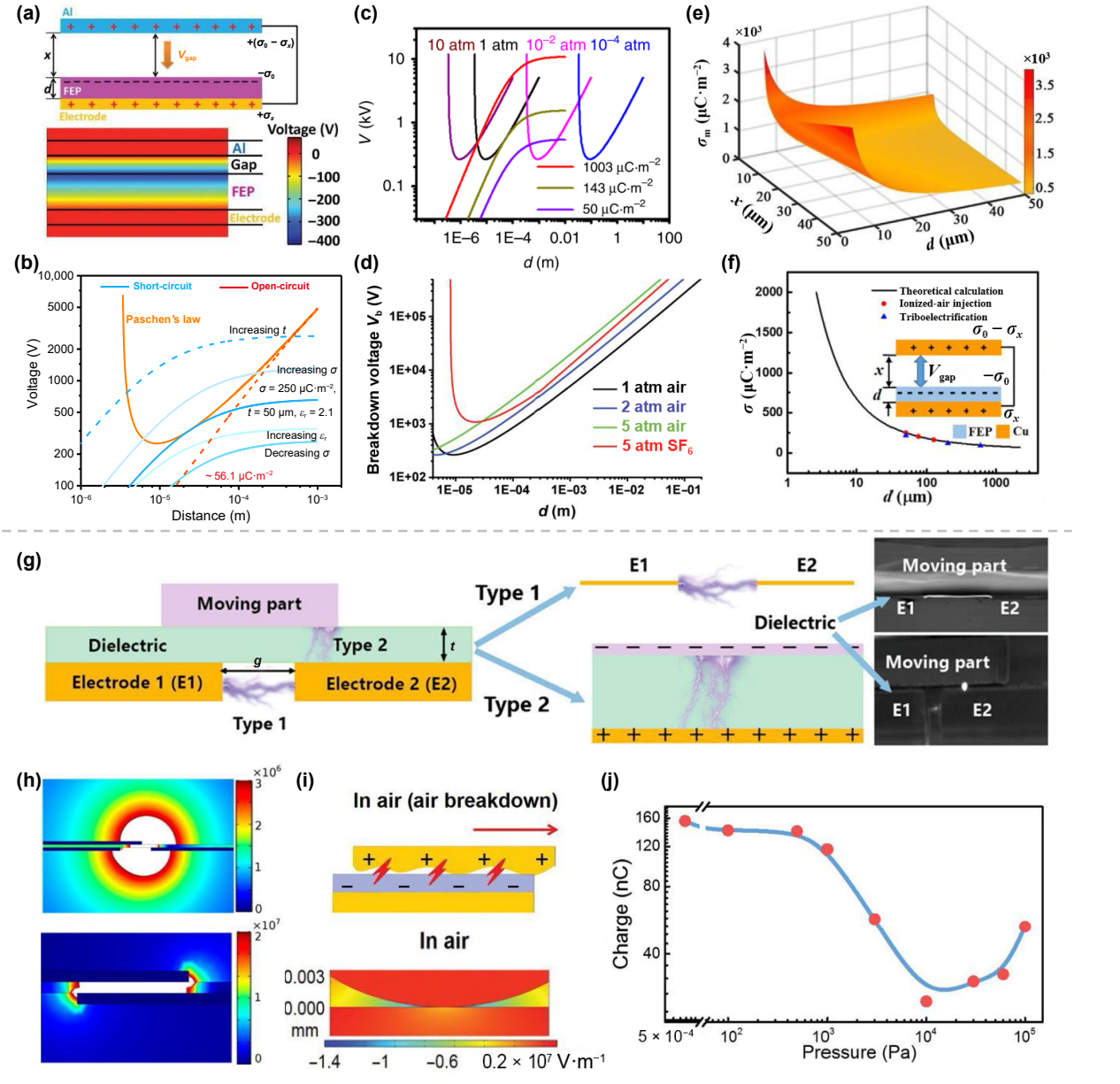

Figure 4 The air breakdown effect in the CS-TENG and sliding mode TENG. (a) The schematic diagram and simulated result of voltage across the air gap in a CS-TENG. Reproduced with permission from Ref. [80], © WILEY-VCH Verlag GmbH & Co. KGaA, Weinheim 2014. (b) The relationship between the air breakdown voltage and the gap voltage at various distances. Reproduced with permission from Ref. [81], © Liu, D. et al. 2022. (c) The relationship between the air breakdown voltage and the gap voltage at various gas pressures. Reproduced with permission from Ref. [79], © Wang, J. et al. 2017. (d) The breakdown voltage of air at different pressures and SF_6 at one atmosphere. Reproduced with permission from Ref. [82], © WILEY-VCH Verlag GmbH & Co. KGaA, Weinheim 2017. (e) The relationship of the theoretical maximum surface charge density, air gap distance, and dielectric thickness. (f) The theoretical maximum surface charge density at different dielectric thicknesses. The inset figure shows the structure of the CS-TENG and corresponding structural and electrical parameters. Reproduced with permission from Ref. [83], © Elsevier Ltd. 2019. (g) Two breakdown types in the sliding mode TENG. (h) Simulated voltage distribution in the sliding mode TENG. Reproduced with permission from Ref. [84], © American Chemical Society 2019. (i) Schematic diagram and the simulated electric field show the air breakdown phenomenon at the sliding interface. (j) Output charges of sliding mode TENG at various air pressures. Reproduced with permission from Ref. [56], © Wiley-VCH GmbH 2020.

for TENGs [85]. However, because of the complex environment involving gas breakdown between two triboelectric layers and environmental factors such as humidity and gas molecules, the triboelectric performance in this series is still environmentally dependent. This pioneering work inspired the combination of the TENG technique and vacuum environment, and an updated triboelectric series was developed in 2022 to understand the maximum TECD of various materials (Fig. 5) [81]. With the air breakdown and environmental factors avoided as much as possible, the vacuum TECD could reflect the intrinsic material properties. This work also shows a promising direction to optimize the performance of triboelectric behaviors by considering triboelectric material pairs rather than one dielectric material.

Surface physical modification is often regarded as an effective method to improve the surface charge density by increasing the real contact area (Figs. 6(a) and 6(b)) [86]. For instance, with patterned arrays (line, cubic, and pyramid) on the surface of the polymer materials, the CS-TENG with pyramid arrays has the highest output performance [44]. In addition, some studies have reported that the surface curvature can affect the triboelectric performance [87]. The detailed mechanism still needs to be revealed with controlled and advanced interface characterization techniques.

Surface chemical modification is a simple and direct way to effectively improve the triboelectric performance of any material in theory by introducing high positive or negative functional groups on the triboelectric surface. In 2016, Wang et al. used thiol molecules with different head groups to modify the Au surface

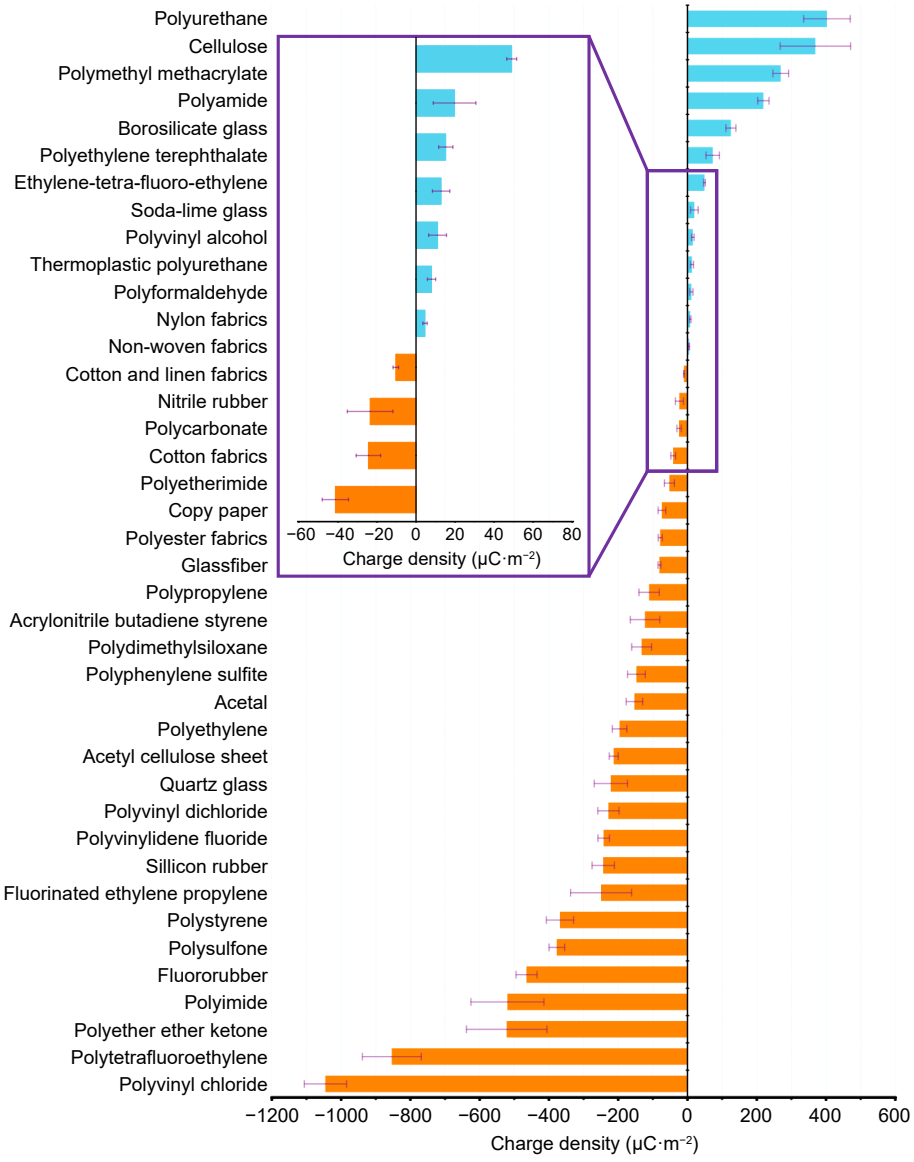

Figure 5 Quantified vacuum triboelectric charge density. Reproduced with permission from Ref. [81], © Liu, D. et al. 2022.

and silane molecules for dielectric surfaces (SiO_2) based on the method of self-assembly monolayers. With amines as the head groups, the surface chemical potential was altered, and the output performance was greatly enhanced [88]. After that, many functional groups, such as poly-L-lysine, 1H,1H,2H,2H-perfluorooctyl-chlorosilane (FOTS), 3-aminopropyltriethoxysilane (APTES), 3-glyci-doxypropyltrie thoxysilane (GPTES), and trichloro(3,3,3-triflfluoropropyl)silane (TFPS), were introduced on the triboelectric surface to improve the triboelectric performance [89–91]. The common consensus is that fluorine and helium atoms tend to gain electrons, while the amino group tends to lose electrons. Recently, by choosing several polymers with similar main chains and modified with different functional groups, the results show that the electron-withdrawing (EW) ability and density of these functional groups on the main chain can determine both the surface charge polarity and density (Fig. 6(c)) [47]. The strength of the EW ability of these functional groups follows the order: CH_3 < H < OH < Cl < F. Research on surface chemical modification is still ongoing.

3.2.2 *Structural design*

The comprehensive performance of TENGs, such as volume density and efficiency, can be optimized by reasonably designed structures, which can also improve the output charge density. With the soft material and fragmental structure design, Wang et al. proposed a tube-like TENG involving silicone rubber as the triboelectric layer and a mixture of silicone rubber and carbon black as the electrode, and a high charge density up to 250 μC·m^{-2} was realized owing to the increased contact intimacy (Fig. 6(e)) [49]. A three-layer structure of the CS-TENG can also improve the charge density to 275.44 μC·m^{-2} relying on the efficient charge separation in the middle layer (Fig. 6(d)) [92]. Developing the new structure of TENGs is particularly important not only to realize high output charge density but also to promote practical applications of TENGs in different scenarios.

3.2.3 *Environmental control*

The surface charges on the dielectric layer could be influenced by environmental factors such as atmospheric pressure, gas composition, temperature, and humidity. In other words, the surface charge density could also be improved by controlling the environment. Generally, the surface charge density in the CS-TENG builds a high electrostatic field across the air gap when the two triboelectric layers are separated, and some surface charges are released by the air breakdown effect. A high vacuum environment can avoid the charge loss from air breakdown, leading to a high charge density of 1003 μC·m^{-2} with the polytetrafluoroethylene (PTFE) and $BaTiO_3$ ferroelectric materials (Fig. 6(f)) [79]. In

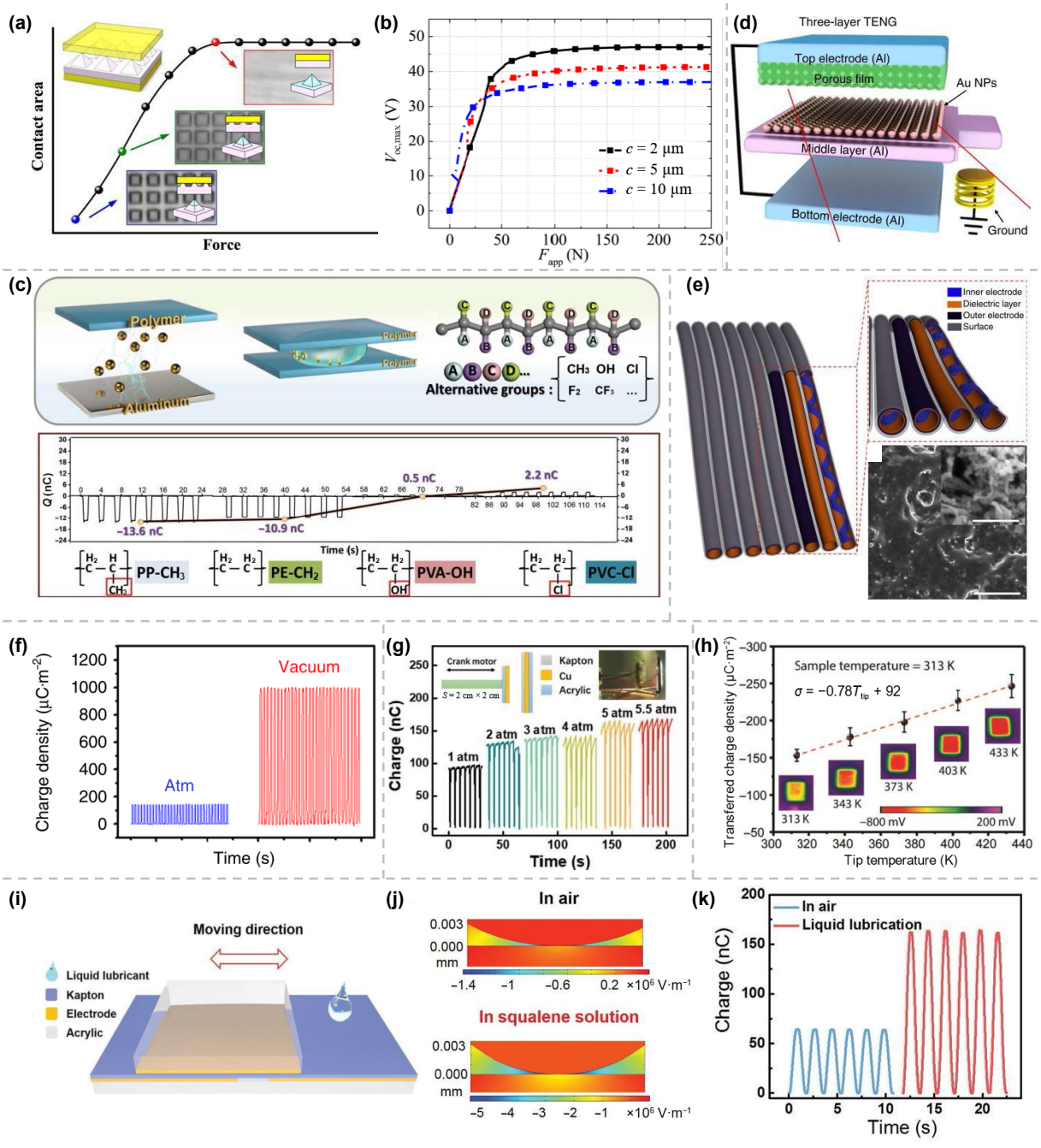

Figure 6 Methods for improving the charge density of TENGs. (a) The relationship between the contact area and the applied force. (b) The open-circuit voltage of the TENG at various forces. This indicates that the charge density can be improved by increasing the contact area. Reproduced with permission from Ref. [86], © Elsevier Ltd. 2018. (c) Surface chemical modification to optimize the surface charge density. Reproduced with permission from Ref. [47], © WILEY-VCH Verlag GmbH & Co. KGaA, Weinheim 2020. (d) With the three-layer structure rather than the two-layer structure to optimize the output charge density. Reproduced with permission from Ref. [92], © Chun, J. S. et al. 2016. (e) Soft and fragmental contact to enhance the surface charge density. Reproduced with permission from Ref. [49], © Wang, J. et al. 2016. (f) Decreasing the pressure to vacuum conditions to optimize the surface charge density. Reproduced with permission from Ref. [79], © Wang, J. et al. 2017. (g) Increasing the air pressure to enhance the surface charge density. The inset figures show the structural diagram and a photo of the tested device. Reproduced with permission from Ref. [93], © Fu, J. J. et al. 2020. (h) Controlling the temperature difference between two materials to optimize the transferred charge density. Reproduced with permission from Ref. [94], © WILEY-VCH Verlag GmbH & Co. KGaA, Weinheim 2019. (i) Schematic diagram showing the liquid lubrication method to increase the surface charge density. (j) The simulated electric field distributions in air and squalene solution. (k) The output charge of the TENG in air and under liquid lubrication. Reproduced with permission from Ref. [56], © Wiley-VCH GmbH 2020.

addition, Zi et al. investigated the output performance of TENGs at various atmosphere pressures and demonstrated enhanced charge density in a high atmosphere pressure environment owing to the restricted air breakdown effect (Fig. 6(g)) [93]. Similarly, the breakdown-resistant gas environment also permits a higher surface charge density.

Increasing the temperature would facilitate the surface charge dissipation caused by the thermionic emission effect. However, some works reported that the output charge density could be improved by increasing the temperature difference between the two contact triboelectric layers [94, 95]. In 2019, Lin et al. revealed that hotter solids tend to receive positive triboelectric charges, while cooler solids tend to be negatively charged in metal and inorganic triboelectric material pairs at the nanoscale by using AFM and KPFM (Fig. 6(h)) [94]. The transferred charge density between two solid materials can be tuned by regulating the temperature difference. This was followed in 2021 by a macroscopic experiment that involved metal and organic

triboelectric material pairs in a CS-TENG, and the surface charge density increased 3 times when the temperature difference increased from 0 to 145 K, providing a method to enhance the output performance of TENGs in high-temperature environments [96].

Furthermore, humidity can also alter the surface condition, affecting the charge transfer behavior, increasing the surface conductivity, and accelerating the charge loss. The air breakdown process could still be modulated under different humidity conditions. Previous works show that the output charge density tends to decline with increasing humidity, and a high output charge density can be achieved in an environment as dry as possible [97]. Recently, Liu et al. revealed that ions are more stable than electrons on the dielectric surface in a high humidity environment, and then the TENG with large amounts of ions on its surface shows high and stable output performance compared with the TENG with large amounts of electrons [98]. Given the simultaneous effects of humidity on charge transfer and charge loss, the mechanism of humidity on the performance of TENGs still needs to be further studied.

3.2.4 *Ultrathin dielectric layer*

The ultrathin dielectric layer in the CS-TENG can greatly decrease the voltage across the air gap when the two triboelectric layers are separated. The first work on the concept of "ultrathin dielectric layers" in CS-TENGs, which utilized the ion injection method to produce surface charges, was reported in 2014 [80]. The existence of maximum surface charge density in the CS-TENG was demonstrated, and the thinner dielectric layer is favorable for higher output charge density. This work was followed by Zhang et al. in 2020, and the basic theory of the limiting factors of maximum surface charge density was rebuilt [83]. With an FEP film of 15 μm, a high surface charge density of 735 $\mu C \cdot m^{-2}$ was obtained directly from triboelectrification under atmospheric conditions. These works provide an effective and promising methodology for improving the charge density of CS-TENGs. Developing advanced dielectric materials with a small thickness (or high relative permittivity) and low leakage current is critical for an efficient TENG.

3.2.5 *Liquid lubrication*

The concept of "liquid lubrication" is commonly utilized for sealing and lubrication between two moving parts in the machinery field. In 2020, Wu et al. introduced liquid lubrication into a sliding mode TENG to reduce material wear and extend the stability of the TENG [99]. Zhou et al. analysed the effect of various liquid species on the performance of several sliding-mode TENGs in detail, and the results show that the output performance of TENGs with squalane as the liquid lubricant is the highest [56]. The improved charge density is attributed to the suppression of air breakdown in the microgap between the triboelectric layer and electrode (Figs. 6(i)–6(k)). The sliding mode TENG with liquid lubrication also exhibits excellent output durability after more than 500,000 working cycles. Overall, the air breakdown in the microgap between the two triboelectric layers of the sliding mode TENG can be restricted by adding the proper liquid lubricant or reducing the surface roughness.

Moreover, the ion or electron injection is also an effective method to improve the surface charge density in the triboelectric layer, which has also been widely used in many previous works [80, 83]. The problem of charge decay should be carefully considered.

3.3 Challenge the charge density limitations

Various methods have been cultivated to improve the charge density of TENGs in the past ten years, but the highest value of the charge density is still approximately 1000 $\mu C \cdot m^{-2}$ [79]. How to improve the charge density to a higher value? Generally, the surface charge density of a TENG is restricted by the air breakdown effect. When the TENG is applied in a high vacuum environment with the avoidance of air breakdown, the surface charge density can be improved. Then, the triboelectrification and dielectric breakdown effects are the next limitations to realizing a high surface charge density. The previous work in a high vacuum environment implies that dielectric breakdown would be the next limiting factor, because the electric field across the dielectric layer is very close to the dielectric breakdown field strength of the dielectric material of PTFE. Developing advanced dielectric materials with a high dielectric breakdown field strength is one of the potential directions to challenge the limitations of dielectric breakdown or triboelectrification. In addition, the vacuum provides an ideal environment to find the next ceiling of surface charge density.

The charge pump technique (or charge excitation strategy), which can be simply understood as utilizing the high output voltage of a pump TENG to charge a large capacitor as the main TENG, is an efficient method enabling a high effective surface charge density. The first charge pump TENG was reported in 2018 by Xu et al. and Cheng et al. in two independent groups (Figs. 7(a)–7(d)) [46, 48]. Because the pump TENG with high output voltage can easily charge the main TENG to a high voltage stage, the capacitance of the main TENG can be dramatically increased with the thinner dielectric layer or larger relative permittivity of the dielectric layer, namely, the charge pump TENG can break through the triboelectrification limitation. Thus, a very high effective surface charge density up to 1020 $\mu C \cdot m^{-2}$ was realized under atmospheric conditions. In 2019, the external-charge-excitation TENG (ECE-TENG) and the self-charge-excitation TENG (SCE-TENG) were proposed by Liu et al. (Figs. 7(e) and 7(f)) [50]. With the help of the voltage multiple circuit (VMC), the effective surface charge density can be increased to 1.25 $mC \cdot m^{-2}$ with a 5 μm Kapton film. In addition, a suitable Zener diode with a certain breakdown voltage is very useful to avoid air breakdown in the main TENG, leading to a more stable output performance. It is worth noting that the special breakdown voltage of the Zener diode should be carefully chosen to maximize the final effective surface charge density. With the carbon/silicone gel electrode to increase contact efficiency, the effective surface charge density increases to 2.38 $mC \cdot m^{-2}$ with the 4 μm polyimide (PI) film (Figs. 7(g) and 7(h)) [100]. Li et al. reported an effective strategy to realize a high charge density of 2.2 $mC \cdot m^{-2}$ by using a fast charge accumulation process on dielectric material with high relative permittivity (Figs. 7(i) and 7(j)) [101]. Then, this value was improved to 3.53 $mC \cdot m^{-2}$ by using a composite film coupling lead zirconate titanate and poly(vinylidene fluoride) with a high relative permittivity [51]. Moreover, in a noncontact mode in air or oil conditions, the charge pump TENG can still realize a high output charge density with a high stability simultaneously (Figs. 7(k)–7(m)) [102, 103], providing great potential for practical applications even in high humidity conditions.

Overall, the vacuum technique combined with advanced triboelectric materials and the charge pump technique combined with advanced dielectric materials could be potential directions to challenge the charge limitations for TENGs. In addition to more focus on negative triboelectric materials, advanced positive triboelectric materials still need to be exploited to form triboelectric material pairs to maximize the charge density. The direct-current TENGs from the electrostatic breakdown effect [104–113] and tribovoltaic effect [114–116] also show the

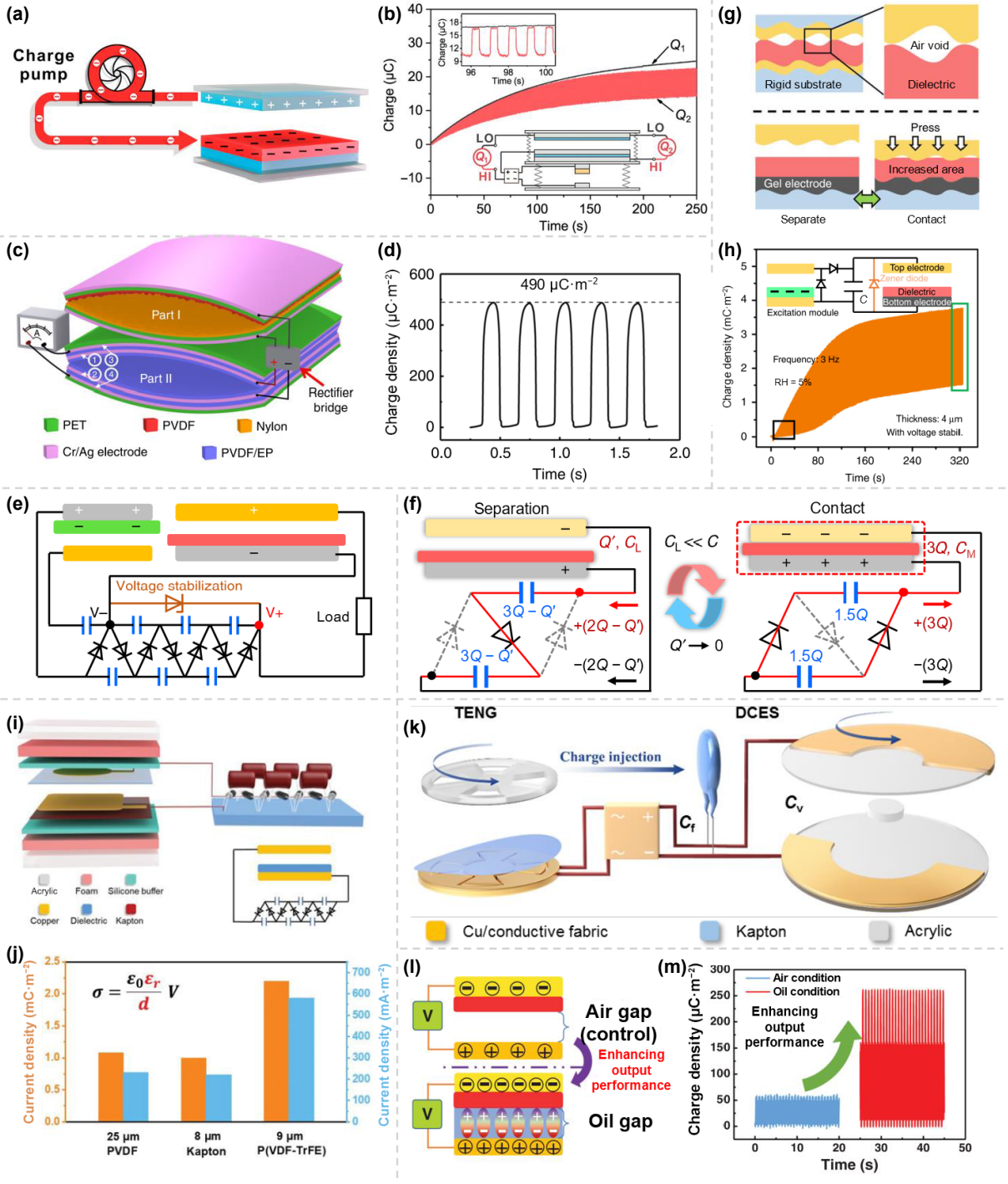

Figure 7 Challenge the limitation of output charge density by the charge pump technique. (a) The diagram of the charge pump. (b) The accumulated output charge with the charge pump technique. The inset figures show the enlarged view and the measurement circuit, where HI and LO mark the "input high" and "input low" terminals of the electrometer respectively. Reproduced with permission from Ref. [46], © Elsevier Ltd. 2018. (c) The two parts in the charge pump TENG with a rectifier. (d) The output charge density of the charge pump TENG. Reproduced with permission from Ref. [48], © Cheng, L. et al. 2018. (e) Combination of the charge pump TENG and the VMCs. (f) The working mechanism of the self-excited charge pump TENG. Reproduced with permission from Ref. [50], © Liu, W. L. et al. 2019. (g) Diagram of the effectiveness of contact in rigid and soft substrates. (h) The output charge density. The inset figure shows the structure of ECE-TENG and the measured circuit. Reproduced with permission from Ref. [100], © Liu, Y. K. et al. 2020. (i) Schematic diagram showing the self-excited charge pump TENG. (j) The output charge density with different dielectric materials. Reproduced with permission from Ref. [101], © Wiley-VCH GmbH 2021. (k) Diagram of the dual capacitor system to boost output charges. Reproduced with permission from Ref. [102], © Wiley-VCH GmbH 2021. (l) The noncontact TENG in air and oil conditions. (m) The charge density of the charge pump TENG in air and oil conditions. Reproduced with permission from Ref. [103], © Wiley-VCH GmbH 2022.

potential to realize a very high effective charge density, which can be found in recent reviews [117, 118].

4 Improving output voltage

The high output voltage is the most prominent characteristic of TENGs, which endows TENGs with promising applications in high-voltage instruments, electrostatic actuators, environmental governance, and intelligent agriculture as a high voltage power source with the merits of portability, controllability, safety, efficiency, and without an additional power supply. The output voltage of the TENG varies with its structure and working mode. This part considers the output voltage characteristics and methods

to improve the output voltage of CS mode TENGs and sliding mode TENGs.

4.1 Output voltage of CS-TENGs

The CS-TENG consists of a variable air capacitor and a constant dielectric capacitor connected in series, and the capacitances in the contact state and separate state are different, leading to the asymmetric voltage of the CS-TENG in the separating process and contacting process. In 2020, Wang et al. systematically studied the mechanism of the asymmetric output voltage of CS-TENGs (Fig. 8(a)) [119]. With a half-wave circuit forwards and backwards connected between two electrodes, the separate-to-contact voltage (V_t) and contact-to-separate voltage (V_d) can be measured integrated with a mechanical switch (Fig. 8(b)). More importantly, V_t is closely related to the dielectric capacitance (C_t), while V_d is closely related to the air capacitance (C_d). Therefore, V_t can be regulated by increasing the thickness and area of the dielectric layer, and V_d can be improved by increasing the separation distance between the two triboelectric layers and the area of the dielectric layer (Figs. 8(c)–8(f)). In addition, increasing the charge density can elevate both V_t and V_d. A high voltage of 16.5 kV was achieved in a CS-TENG with an electrode area of 100 cm^2 and a PTFE thickness of 0.1 mm.

Using a half-wave circuit connected in parallel with the TENG to form a charge supplement channel is a facile technique to realize a high output voltage. In 2018, Xu et al. reported that the open-circuit voltage of a TENG increases from 230 V to more than 3300 V over ten times by introducing the charge supplement channel (Figs. 8(g)–8(i)) [120]. This method has been widely used in many recent works to build a high voltage and then combined with a spark switch to maximize the energy output from TENGs [121, 122].

The development of layered CS-TENGs greatly increases the power density per unit volume, facilitating their wide application in motion energy and wave energy harvesting. As the output voltage of the TENG is easily affected by the parasitic capacitor [53], generally a negative effect, the symmetrical stacked structure of the layered CS-TENG will produce a high output voltage, while the alternative stacked structure of the layered CS-TENG has a low output voltage because of the extra parasitic capacitor between the two adjacent TENGs resulting from reversed output polarity (Figs. 8(j)–8(m)). In other words, the output voltage of the layered

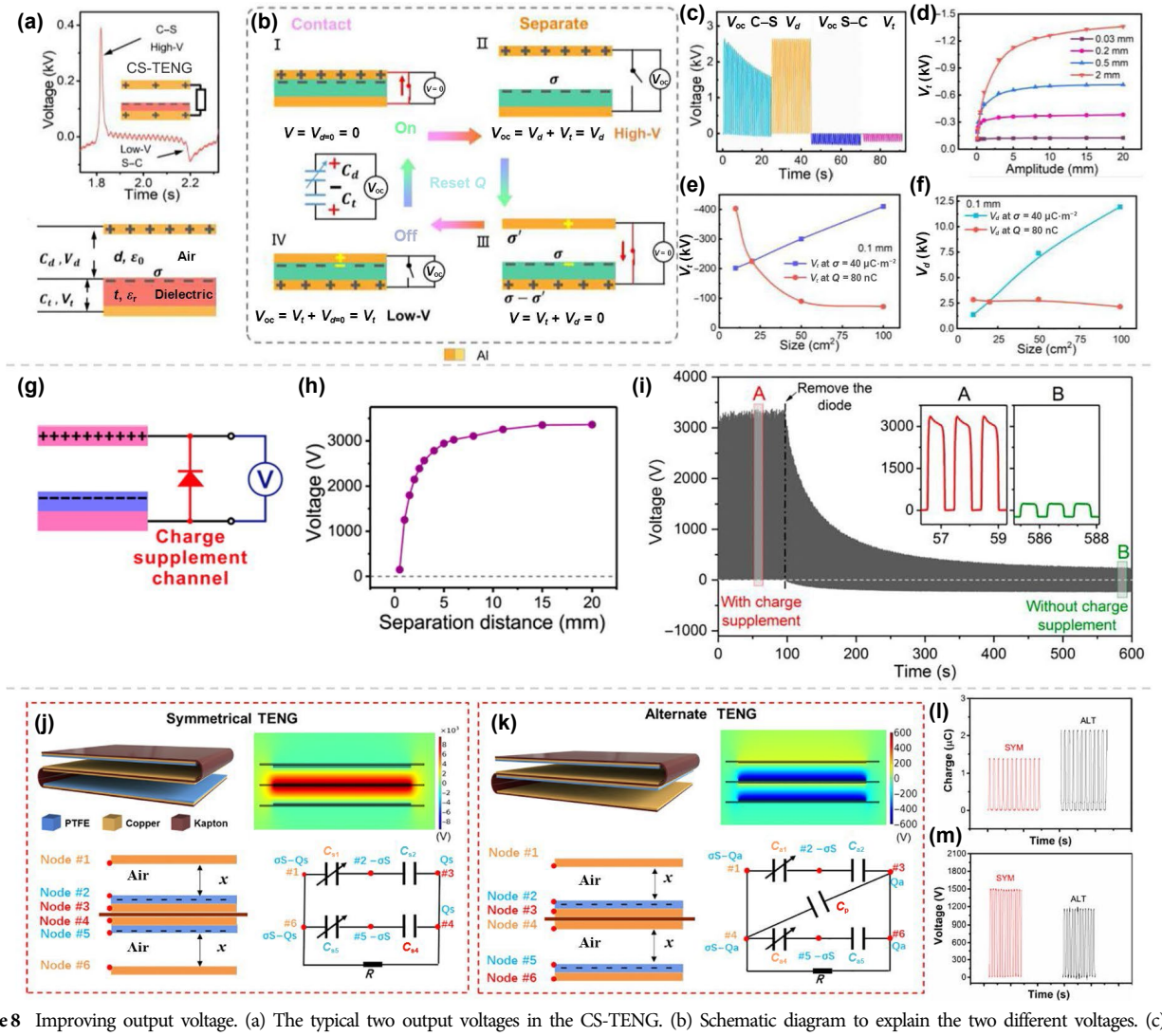

Figure 8 Improving output voltage. (a) The typical two output voltages in the CS-TENG. (b) Schematic diagram to explain the two different voltages. (c) The different output voltages in a CS-TENG. (d) The contact voltages of the CS-TENGs with different dielectric thicknesses. (e) The contact voltages of CS-TENGs with different sizes. (f) The separate voltages of CS-TENGs with different sizes. Reproduced with permission from Ref. [119], © Elsevier Ltd. 2020. (g) Diagram of voltage improvement in a CS-TENG by a half-wave circuit. (h) The output voltage at various separation distances. (i) The output voltages with the charge supplement channel and without the charge supplement channel. Reproduced with permission from Ref. [120], © American Chemical Society 2018. (j) The structure, simulated voltage distribution, and equivalent electric circuit of the symmetrical laminated TENG. (k) The structure, simulated voltage distribution, and equivalent electric circuit of the alternate laminated TENG. (l) The output charges of the symmetrical (SYM)-TENG and alternate (ALT)-TENG. (m) The output voltages of the SYM-TENG and ALT-TENG. Reproduced with permission from Ref. [53], © American Chemical Society 2018.

CS-TENG can be improved by adopting the symmetrical stacked structure and increasing the device area to reduce the parasitic capacitance.

4.2 Output voltage of sliding mode TENGs

Different from the output voltage characteristics of CS-TENGs, the output voltage of sliding mode TENGs is symmetrical when the sliding part moves in and out. In a FT-TENG, where two stationary electrodes were placed at the stator, a charged triboelectric layer induced periodic changes in the induced potential between the two electrodes, driving the charges flowing in the external circuit. The measured open-circuit voltage is extremely high and over 10 kV in a small area of 7 cm × 5 cm, and the simulated open-circuit voltage even surpasses 200 kV when the distance between the two stationary electrodes is 5 cm [52]. The difference between the measured and simulated values could be attributed to the non-ideal measurement condition that the internal resistance of the electrometer is not infinitely large, and the parasitic capacitance cannot be ignored. Moreover, the output voltage of the FT-TENG is not insensitive to the vertical distance of the moving triboelectric layer and the stator, which is very useful for designing a noncontact mode FT-TENG for practical applications. Overall, the output voltage of the FT-TENG can be improved by increasing the distance between the two stationary electrodes and the device area.

Furthermore, the use of a charge accumulation strategy to replenish the charge leakage from the accumulators has improved the output voltage of the rotary mode TENG, and a sustainable ultrahigh voltage of approximately 20 kV was realized by employing the mechanical switch [54]. The small inherent capacitance between the two accumulators supports high voltage production.

4.3 Challenge the voltage limitations

The general methods for improving the output voltage of TENGs mainly rely on increasing the surface charge density, decreasing the inherent capacitance within the TENG, and increasing the device area. There is no doubt that the voltage can be improved along these directions. By employing advanced methods to enhance the charge density, such as material optimization, high vacuum conditions to avoid air breakdown, and breakdown-resistant gas conditions and liquid lubrication methods to restrict the air breakdown effect, the output voltage can be improved to a high level. In addition, previous works indicate that the output voltage of TENGs cannot be continuously improved by decreasing the inherent capacitance within the TENG. Because the reduced inherent capacitor amplifies the effect of the parasitic capacitor on the performance of the TENG [123], the latter greatly restricts the maximum output voltage. It is noted that a large inherent capacitor is beneficial for realizing the high output charges and reducing the effect of parasitic capacitor, while a small inherent capacitor is beneficial for realizing the high output voltage and increasing the effect of parasitic, which seems to be carefully considered for maximizing output energy density, and this will be discussed in the next part. Overall, reducing the impact of parasitic capacitance on output voltage is especially critical to challenge voltage limitations.

The half-wave circuit has been successfully applied in the CS-TENG to realize a high contact-to-separate voltage by forming a charge supplement channel, which is higher than the output voltage of a common CS-TENG [119–122]. Similarly, a charge accumulation strategy was used in a rotary mode TENG to achieve a sustainable high voltage [124, 125]. The "charge supplement" idea seems to be a promising and simple method to address voltage limitations.

VMCs were applied in the CS-TENG, rotary mode TENG, and charge pump technique to increase the output voltage in multiples, which have been successfully used for electrostatic spinning [54] and plasma generation [40]. In principle, the output voltage after VMCs can be linearly increased by increasing the unit VMC, which provides a simple and effective method to improve the output voltage and challenge the voltage limitations.

5 Improving energy density

Energy density (also named average power density) describes the output energy of the TENG (the enclosed area of the V–Q curve) per unit area or volume [77], which is also considered a standardized parameter to quantify the output capability of the TENG.

5.1 Improving charges and voltage

Obviously, the output energy density of the TENG can be improved by increasing the output charges and output voltage, i.e., maximizing the enclosed area of the V–Q curve. Great efforts have been devoted to this research, and the output energy density of TENGs has been greatly improved in the last ten years. Especially in recent years, the output energy density of TENGs has been elevated to a very high value, which could even be comparable with the value of solar cells [37]. In 2020, a rationally designed shielding layer and alternative tribo-black-area were introduced into sliding mode TENGs to restrict the air breakdown effect in the triboelectric layer and to accelerate the charge accumulation on the triboelectric area, respectively (Figs. 9(a) and 9(b))[55]. In addition, the facilitated charge dissipation in the black area is also beneficial for charge accumulation in the triboelectric area, finally enabling a high average power density of 1.3 $W{\cdot}m^{-2}{\cdot}Hz^{-1}$ at an external load of 250 MΩ (Fig. 9(c)). Meanwhile, by introducing the liquid lubricant of squalane into the triboelectric surface [56], the air breakdown in the triboelectric surface can be greatly restricted, and the output charges and voltage were dramatically improved, leading to a high average power density of 3.45 $W{\cdot}m^{-2}{\cdot}Hz^{-1}$ at an external load of 5 MΩ (Figs. 9(d) and 9(e)). This method is simple and universal for any sliding mode TENG.

In 2021, Wu et al. reported an opposite-charge-enhanced transistor-like TENG (OCT-TENG) composed of coplanar tribo-surfaces with opposite-charge polarization to enhance the charge transfer, and a high average power density up to 0.79 $W{\cdot}m^{-2}{\cdot}Hz^{-1}$ was achieved at an external load of 10 MΩ (Figs. 9(f)–9(h)) [36]. Recently, combined with the charge space-accumulation effect, liquid lubrication, and voltage balance (VB) bar design, He et al. reported a sliding TENG enabling an average power density of 87.26 $W{\cdot}m^{-2}{\cdot}Hz^{-1}$ (Figs. 9(i)–9(m)) [37]. With a palm-sized device working at 120 rpm, a cell phone can be charged to turn on within 25 s, exhibiting the promising applications of TENGs as self-powered sources.

5.2 Employing the diode and switch

In 2015, Zi et al. first proposed employing the V–Q curve to describe the output energy density of a TENG [77]. It is predicted that the maximized output energy density could be obtained at an infinite external load resistance, and a motion-triggered mechanical switch was connected in parallel with a sliding mode TENG to maximize the transferred charges, enabling a high output energy density. This was followed by Cheng et al. in 2017 by employing a series connected switch with the TENG. The switch will turn on only when the maximum voltage of the TENG is reached, and a maximum energy output can be obtained regardless of the external load resistance value [126]. Similarly, the half-wave circuit can also reset the charge distribution in two

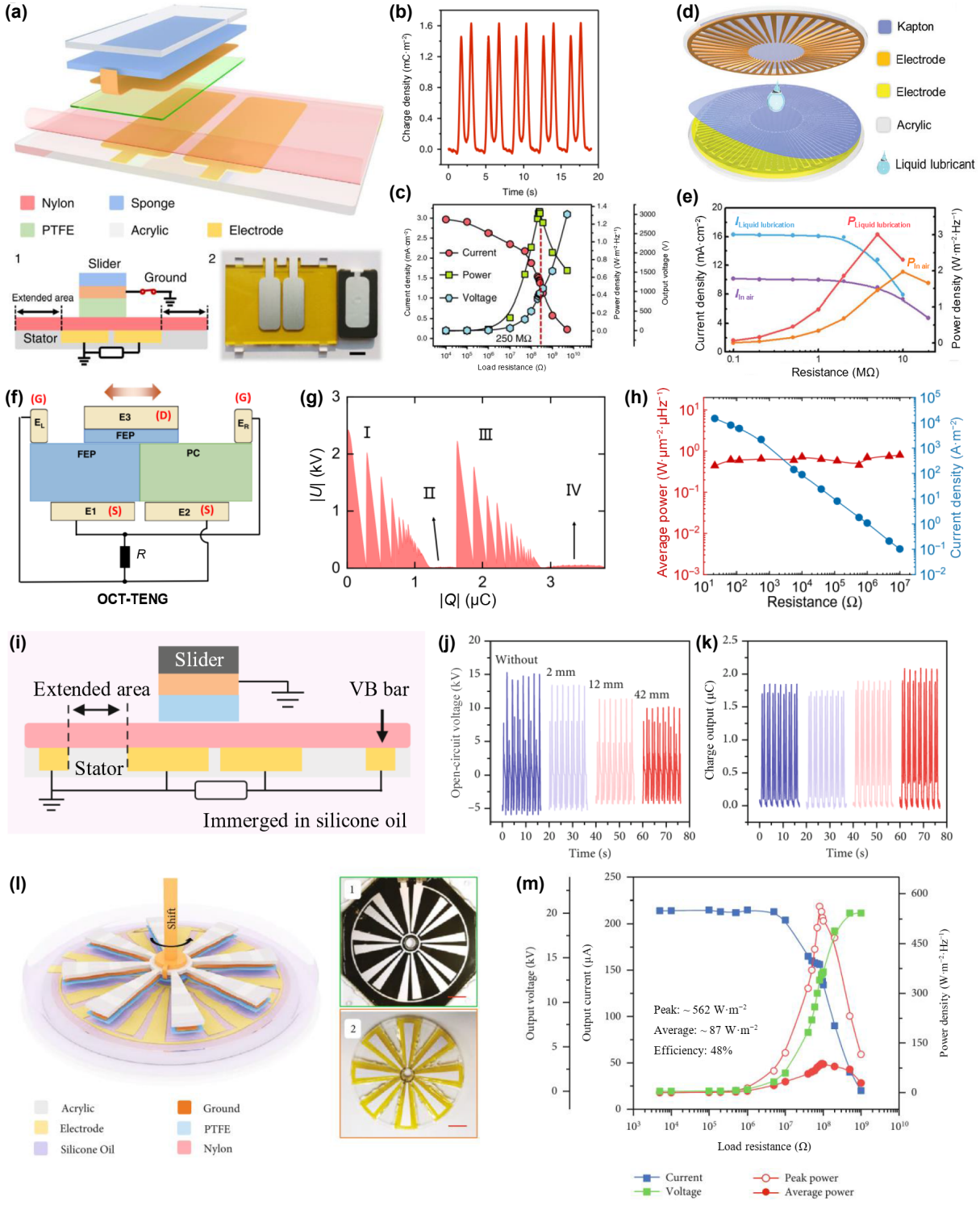

Figure 9 Improving output energy. (a) The sliding mode TENG with two extended areas in the stator to boost the output charge. (b) The output charge density. (c) The output current density, voltage, and power density with various load resistances. Reproduced with permission from Ref. [55], © He, W. C. et al. 2020. (d) Diagram of using liquid lubrication to enhance the output charge density. (e) The output current density and power density at various load resistances. Reproduced with permission from Ref. [56], © Wiley-VCH GmbH 2020. (f) Diagram of the OCT-TENG. (g) The output voltage and charge curves. (h) The output current density and average power of the OCT-TENG at various resistances. Reproduced with permission from Ref. [36], © Wu, H. et al. 2021. (i) Diagram of a sliding mode TENG with an extended area and voltage balance bar to boost the output charge. (j) The open-circuit voltages without the VB bar and with VB bars of different lengths. (k) The output charges without the VB bar and with VB bars of different lengths. (l) The rotary sliding mode TENG. (m) The output voltage, current, and power density of the rotary sliding mode TENG at various load resistances. Reproduced with permission from Ref. [37], © He, W. C. et al. 2022.

electrodes and solve the asymmetry problem in the CS-TENG, enabling maximum energy output [119, 127]. Recently, an auto-switched system comprised a half-wave circuit, an input capacitor, a voltage-controlled switch, and a CS-TENG, promises to generate a stable high voltage; it thus exhibits a very high output energy density up to 142 mJ·m^{-2} with rationally designed spark switches and air gaps, providing very meaningful guidance for future research (Figs. 10(a)–10(e)) [122]. However, to build a stable voltage so high, the surface charge density is restricted by air breakdown at only approximately 50 μC·m^{-2}, so realizing the maximum energy output in the atmosphere is very challenging. The results under high vacuum conditions indicate that a

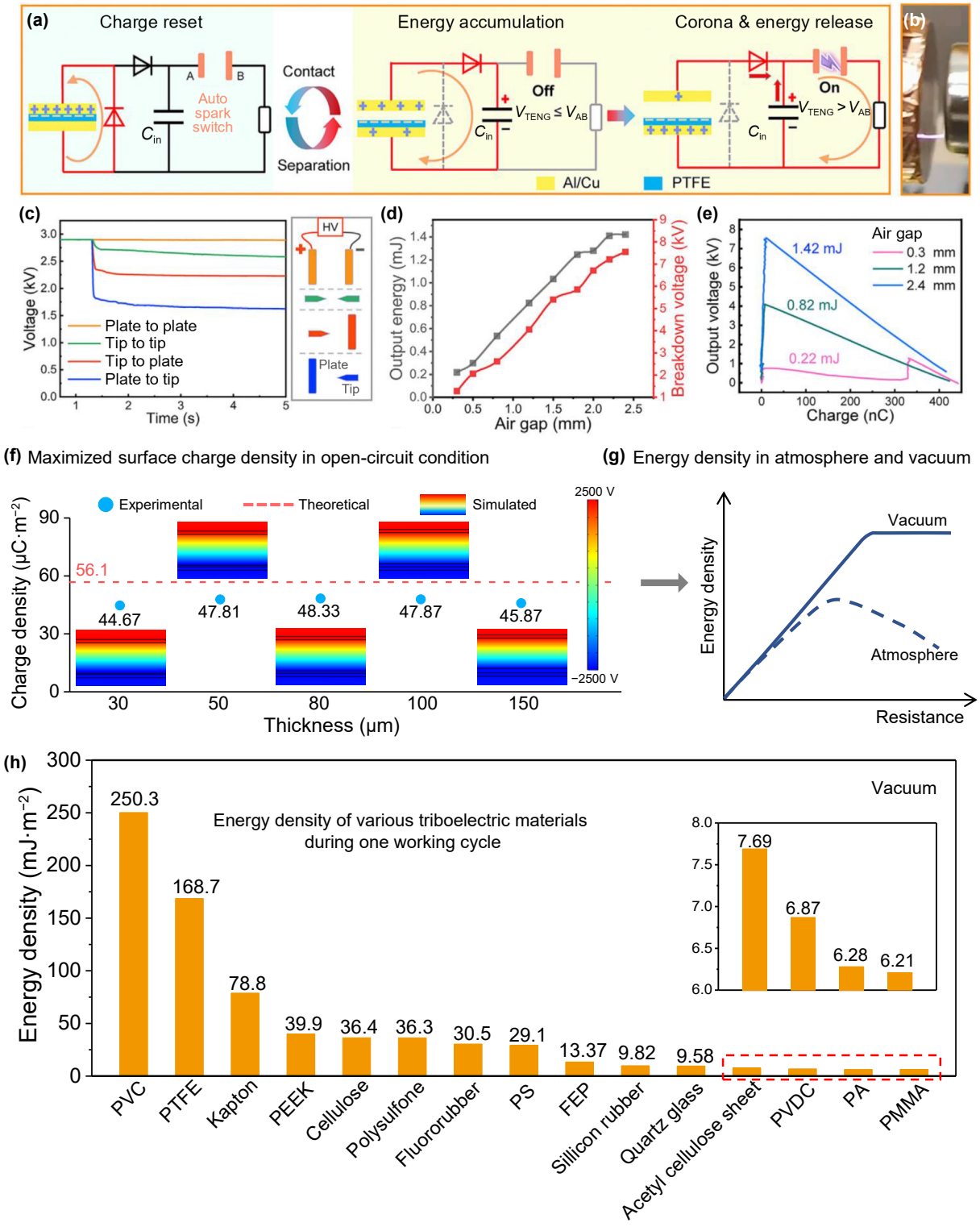

Figure 10 Challenge the limitation of output energy density. (a) The CS-TENG combined with the half-wave circuit and the spark switch to enhance the output energy density. (b) Photograph of the spark switch. (c) The output voltage of different spark switches (left). The switch designs include plate to plate, plate to tip, tip to plate, and tip to tip (right). (d) The output energy and breakdown voltage at different air gap distances. (e) The output voltage–charge curves with different air gap distances. Reproduced with permission from Ref. [122], © Elsevier Inc. 2020. (f) The maximized surface charge density under open-circuit condition. (g) The diagrams show the energy density in atmosphere and vacuum. (h) The energy density of various triboelectric materials during one working cycle under vacuum condition. Reproduced with permission from Ref. [81], © Liu, D. et al. 2022.

maximum energy density up to 250.3 mJ·m^{-2} can be achieved (Figs. 10(f)–10(h)) [81], which could be further elevated by reducing the effect of parasitic capacitance on the output energy density in the future.

5.3 Challenge the energy density limitations

There is no doubt that the energy density of TENGs can be improved by increasing Q and V according to the energy density definition (or the V–Q plot). However, the breakdown effect in TENGs should be carefully considered. The method, employing the diode and switch (mechanical switch, electric switch, and spark switch) to reset the charge distribution and to build a high voltage realizing energy accumulation, provides promising solutions to maximize the energy extraction from TENGs.

Specifically, the breakdown effect in TENGs is also amplified when a high voltage is applied to the load (the charge distributions in the two electrodes are very different under short-circuit conditions and with a large external load), which must be considered for maximizing energy output. For practical applications, the trade-off between Q and V is essential for maximizing energy output realization. To challenge the energy density limitations, the vacuum environment, high breakdown-resistant gas condition, and liquid lubrication support a higher critical breakdown threshold, which could be potential directions.

Notably, the asymmetric output performance of CS-TENGs in contacting and separating processes has often been neglected. In 2017, Peng et al. proposed a simple model for optimizing triboelectric power generation by matching the device capacitance and external load resistance [128]. When the time-varying resistance–capacitance (RC) product of the TENG better matches the mechanical motion frequency, the power density can theoretically be increased over 10 times. In addition, increasing the device area is an effective method to reduce the effect of parasitic capacitance on the output power of TENGs.

6 Summary and future perspectives

Although TENGs are promising in the new era of IoT, comprehensively improving the performance of TENGs for wide applications remains challenging. Regulating the performance of TENGs at different levels demands advances in various aspects, such as fundamental physics studies of CE, materials development, device design, integration, lifetime, and standard evaluation. Without proper consideration, a high-performance TENG is difficult to deploy for practical applications.

6.1 Fundamental physics of CE

Understanding the fundamental physics of the CE is intrinsically critical for improving the performance of TENGs. Determining the charge transfer species during CE, including electron, ion, and material transfer, is one of the most basic problems in this area. Recent works have demonstrated electron transfer in solid–solid, solid–liquid, and liquid–liquid pairs, while the charge transfer species in gas–solid, gas–liquid, and gas–gas pairs remain to be studied. Specifically, the ratio of transferred electrons to ions varies from the surface hydrophobicity of the solid and the composition of the solution, which still needs more detailed research. Furthermore, the transferred charge quantity in the CE is more important to reflect the output capability of the TENG. Although great efforts have been devoted to improving the triboelectric charge density, the record-high charge density value seems to be stable at approximately the order of 1000 $\mu C \cdot m^{-2}$ (approximately one electron transfer in ten thousand atoms) even under vacuum conditions (avoiding air breakdown) and in liquid–solid pairs (realizing intimate contact). What is the limit value of triboelectrification, and which factors determine the limitations? These issues still need to be explored.

6.2 Charge density improvement

The electric output performance of TENGs is mainly determined by the charge density. Although many methods have been proposed to improve the charge density of TENGs, developing new methods, designing rational structures, and cultivating advanced materials are still needed to further enhance the performance of TENGs, leading to more efficient power sources for power electronics with more power requirements. The charge transfer from triboelectrification is nearly independent of the dielectric thickness, requiring only a few several or hundred nanometers for charge transfer. Thus, the coating of advanced triboelectric materials on the surface of other materials may be a simple but effective method to improve the performance of TENGs and promote their wide application. Special attention must be paid to the preparation process and the combination degree of the hybrid layer to ensure the feasibility and reliability to avoid the failure of advanced triboelectric materials. The emerging charge pump technique and direct current TENGs (arising from the electrostatic breakdown and tribovaltic effects) also provide potential directions to greatly improve the performance of TENGs, which still needs more efforts to be promoted.

6.3 Output voltage improvement

Improving the output voltage and designing the adjustable voltage according to the practical requirement are important to promote the wide applications of TENGs in some special fields. Although many efforts have been devoted to improving the output voltage of TENGs, the output voltage is still limited by the air breakdown effect, leakage current, parasitic capacitance, etc. Specifically, the high output voltage of TENGs always requires a large external load to be connected, which will aggravate the air breakdown effect in TENGs and other exposed tips in air, resulting in the unwanted charge loss and then limiting the output voltage. Therefore, restricting the charge loss into the air (air breakdown) and the dielectric film (leakage current) is an important direction to elevate the output voltage combined with the reduced parasitic capacitance. In addition, employing the half-wave circuit and VMCs is an easy method to realize a high output voltage. Furthermore, exploring the new generation of TENG-based high-voltage power sources with portability, controllability, safety, and high efficiency is promising for the rapid and sustainable development of new high-voltage power sources.

6.4 Lifetime requirement

A reliable TENG should maintain stable performance throughout service. In the last decade, great methods and advanced structures have been demonstrated to enhance the electric performance stability, and the stability of TENGs has been promoted to a high level depending on the different working modes. Reducing the material wear and energy loss in sliding mode triboelectrification is always a troublesome problem. The switchable structure of triboelectric layers in contact and separate states can largely enhance the robustness and durability of sliding mode TENGs. Introducing rationally selected liquid lubricant into triboelectric layers is a promising method to simultaneously enhance the performance and stability of sliding mode TENGs. Developing durable materials is the fundamental method to solve the lifetime problem of sliding mode TENGs. Furthermore, the lifetime requirement of devices working in a practical environment should be considered, because it does not always require long-term durable TENGs in some special conditions. Hence, a trade-off between the device lifetime and the practical requirement is essential for target applications for TENGs. For some special requirements, such as a waterproof and stable atmosphere, developing advanced encapsulation technologies is also critical to realize a stable working environment.

6.5 Integration

Most TENGs produce pulsed alternating current and high output voltage, while electronics often require a constant current with low voltage characteristics. The impedance mismatching problem between the energy supply and energy demand makes it necessary to develop highly efficient power management circuits. As power sources, highly efficient power management circuits, generally composed of a spark switch and matched transformers or

inductors, have been proposed to realize a high energy conversion efficiency. System integration considering miniaturization, cost, and target requirements is essential for wide applications of TENG-based power sources. As self-powered sensors, the integration of multimode TENGs or other sensing components to realize multifunctional sensors should be carefully considered. For example, the special characteristics such as flexibility, comfortability, breathability, and biocompatibility of multifunctional sensors on skin could be the top priority. As blue energy harvesting, the introduction of spring structure and network design can enhance the output energy. Comprehensively considering the integration from structure design and power management to network design at various levels or scales will help to improve the final energy conversion efficiency. As high-voltage power sources, developing advanced structures of TENGs to realize sufficiently high output voltage and combining them with a voltage-adjusted circuit are critical for exaggerating the applications of TENGs as safe high-voltage power sources.

6.6 Standard evaluation

The FOMs for TENGs were first proposed in 2015 to evaluate the output performance of TENGs. It is still very difficult to implement these FOMs in practical conditions at this early stage, because they rely on test conditions such as the external applied force, environmental humidity, and temperature. Standard test conditions, including a stable environment (including atmosphere pressure and composition, humidity, temperature, ambient wind velocity, etc.), mechanical trigger (the magnitude and direction of external force), and movement parameters (velocity, frequency, displacement, etc.) are suggested to be unified for performance comparison. General standards to evaluate the stability and lifetime of TENGs are required owing to the differences in materials, structures, working modes, etc. The measuring methods and instruments for electric performance evaluation of TENGs are often overlooked in previous works. Especially for the instantaneous output current and open-circuit voltage, the internal resistance of the instrument, the ground terminal, the parasitic capacitance, and even the distant substrate are common critical factors that greatly influence the measurement results. Evaluating the total efficiency of TENGs from mechanical energy to electric energy is still challenging because of the complexity of quantifying the mechanical energy source and clarifying the energy destinations. The establishment of performance evaluation and test standards is strongly encouraged and required for guiding the design of TENGs in practical applications, facilitating communication between different research groups, and promoting the industrialization of TENGs.

Acknowledgements

Research was supported by the National Key Research and Development Project from Minister of Science and Technology (No. 2021YFA1201602), the National Natural Science Foundation of China (Nos. U21A20147, 22109013, and 62204017), the China Postdoctoral Science Foundation (No. 2021M703172), the Innovation Project of Ocean Science and Technology (No. 22-3-3-hygg-18-hy), and the Fundamental Research Funds for the Central Universities (No. E1E46802).

References

[1] Wang, Z. L. Entropy theory of distributed energy for internet of things. *Nano Energy* **2019**, *58*, 669–672.

[2] Wang, Z. L. Triboelectric nanogenerators as new energy technology and self-powered sensors—Principles, problems, and perspectives. *Faraday Discuss.* **2014**, *176*, 447–458.

[3] Fan, F. R.; Tian, Z. Q.; Wang, Z. L. Flexible triboelectric generator. *Nano Energy* **2012**, *1*, 328–334.

[4] Zhu, G.; Chen, J.; Zhang, T. J.; Jing, Q. S.; Wang, Z. L. Radial-arrayed rotary electrification for high performance triboelectric generator. *Nat. Commun.* **2014**, *5*, 3426.

[5] Xu, W. H.; Zheng, H. X.; Liu, Y.; Zhou, X. F.; Zhang, C.; Song, Y. X.; Deng, X.; Leung, M.; Yang, Z. B.; Xu, R. X. et al. A droplet-based electricity generator with high instantaneous power density. *Nature* **2020**, *578*, 392–396.

[6] Hinchet, R.; Yoon, H. J.; Ryu, H.; Kim, M. K.; Choi, E. K.; Kim, D. S.; Kim, S. W. Transcutaneous ultrasound energy harvesting using capacitive triboelectric technology. *Science* **2019**, *365*, 491–494.

[7] Dong, Y.; Xu, S. W.; Zhang, C.; Zhang, L. Q.; Wang, D. A.; Xie, Y. Y.; Luo, N.; Feng, Y. G.; Wang, N. N.; Feng, M. et al. Gas–liquid two-phase flow-based triboelectric nanogenerator with ultrahigh output power. *Sci. Adv.* **2022**, *8*, eadd0464.

[8] Li, Y. H.; Zhao, Z. H.; Gao, Y. K.; Li, S. X.; Zhou, L. L.; Wang, J.; Wang, Z. L. Low-cost, environmentally friendly, and high-performance triboelectric nanogenerator based on a common waste material. *ACS Appl. Mater. Interfaces* **2021**, *13*, 30776–30784.

[9] Guo, H. Y.; Pu, X. J.; Chen, J.; Meng, Y.; Yeh, M. H.; Liu, G. L.; Tang, Q.; Chen, B. D.; Liu, D.; Qi, S. et al. A highly sensitive, self-powered triboelectric auditory sensor for social robotics and hearing aids. *Sci. Robot.* **2018**, *3*, eaat2516.

[10] Li, S. X.; Zhao, Z. H.; Liu, D.; An, J.; Gao, Y. K.; Zhou, L. L.; Li, Y. H.; Cui, S. N.; Wang, J.; Wang, Z. L. A self-powered dual-type signal vector sensor for smart robotics and automatic vehicles. *Adv. Mater.* **2022**, *34*, 2110363.

[11] Zhang, J. H.; Li, Z. T.; Xu, J.; Li, J. A.; Yan, K.; Cheng, W.; Xin, M.; Zhu, T. S.; Du, J. H.; Chen, S. X. et al. Versatile self-assembled electrospun micropyramid arrays for high-performance on-skin devices with minimal sensory interference. *Nat. Commun.* **2022**, *13*, 5839.

[12] Sun, Z. D.; Zhu, M. L.; Shan, X. C.; Lee, C. Augmented tactile-perception and haptic-feedback rings as human–machine interfaces aiming for immersive interactions. *Nat. Commun.* **2022**, *13*, 5224.

[13] Zhang, Q.; Liang, Q. J.; Nandakumar, D. K.; Qu, H.; Shi, Q. F.; Alzakia, F. I.; Tay, D. J. J.; Yang, L.; Zhang, X. P.; Suresh, L. et al. Shadow enhanced self-charging power system for wave and solar energy harvesting from the ocean. *Nat. Commun.* **2021**, *12*, 616.

[14] Zhang, C. G.; He, L. X.; Zhou, L. L.; Yang, O.; Yuan, W.; Wei, X. L.; Liu, Y. B.; Lu, L.; Wang, J.; Wang, Z. L. Active resonance triboelectric nanogenerator for harvesting omnidirectional water-wave energy. *Joule* **2021**, *5*, 1613–1623.

[15] Xu, S. X.; Liu, G. L.; Wang, J. B.; Wen, H. G.; Cao, S.; Yao, H. L.; Wan, L. Y.; Wang, Z. L. Interaction between water wave and geometrical structures of floating triboelectric nanogenerators. *Adv. Energy Mater.* **2022**, *12*, 2103408.

[16] Liang, X.; Jiang, T.; Liu, G. X.; Feng, Y. W.; Zhang, C.; Wang, Z. L. Spherical triboelectric nanogenerator integrated with power management module for harvesting multidirectional water wave energy. *Energy Environ. Sci.* **2020**, *13*, 277–285.

[17] Li, Y. F.; Bouza, M.; Wu, C. S.; Guo, H. Y.; Huang, D. N.; Doron, G.; Temenoff, J. S.; Stecenko, A. A.; Wang, Z. L.; Fernández, F. M. Sub-nanoliter metabolomics via mass spectrometry to characterize volume-limited samples. *Nat. Commun.* **2020**, *11*, 5625.

[18] Yang, H.; Pang, Y. K.; Bu, T. Z.; Liu, W. B.; Luo, J. J.; Jiang, D. D.; Zhang, C.; Wang, Z. L. Triboelectric micromotors actuated by ultralow frequency mechanical stimuli. *Nat. Commun.* **2019**, *10*, 2309.

[19] Li, Q. Y.; Liu, W. L.; Yang, H. M.; He, W. C.; Long, L.; Wu, M. B.; Zhang, X. M.; Xi, Y.; Hu, C. G.; Wang, Z. L. Ultra-stability high-voltage triboelectric nanogenerator designed by ternary dielectric triboelectrification with partial soft-contact and non-contact mode. *Nano Energy* **2021**, *90*, 106585.

[20] Zhou, L. L.; Liu, D.; Li, S. X.; Yin, X.; Zhang, C. L.; Li, X. Y.; Zhang, C. G.; Zhang, W.; Cao, X.; Wang, J. et al. Effective removing of hexavalent chromium from wasted water by

triboelectric nanogenerator driven self-powered electrochemical system—Why pulsed DC is better than continuous DC? *Nano Energy* **2019**, *64*, 103915.

[21] Han, K.; Luo, J. J.; Feng, Y. W.; Xu, L.; Tang, W.; Wang, Z. L. Self-powered electrocatalytic ammonia synthesis directly from air as driven by dual triboelectric nanogenerators. *Energy Environ. Sci.* **2020**, *13*, 2450–2458.

[22] Zhang, S.; Chi, M. C.; Mo, J. L.; Liu, T.; Liu, Y. H.; Fu, Q.; Wang, J. L.; Luo, B.; Qin, Y.; Wang, S. F. et al. Bioinspired asymmetric amphiphilic surface for triboelectric enhanced efficient water harvesting. *Nat. Commun.* **2022**, *13*, 4168.

[23] Huo, Z. Y.; Kim, Y. J.; Suh, I. Y.; Lee, D. M.; Lee, J. H.; Du, Y.; Wang, S.; Yoon, H. J.; Kim, S. W. Triboelectrification induced self-powered microbial disinfection using nanowire-enhanced localized electric field. *Nat. Commun.* **2021**, *12*, 3693.

[24] Zhang, B. F.; Zhang, C. G.; Yang, O.; Yuan, W.; Liu, Y. B.; He, L. X.; Hu, Y. X.; Zhao, Z. H.; Zhou, L. L.; Wang, J. et al. Self-powered seawater electrolysis based on a triboelectric nanogenerator for hydrogen production. *ACS Nano* **2022**, *16*, 15286–15296.

[25] Liu, W. B.; Duo, Y. N.; Liu, J. Q.; Yuan, F. Y.; Li, L.; Li, L. C.; Wang, G.; Chen, B. H.; Wang, S. Q.; Yang, H. et al. Touchless interactive teaching of soft robots through flexible bimodal sensory interfaces. *Nat. Commun.* **2022**, *13*, 5030.

[26] Zhu, M. L.; Sun, Z. D.; Chen, T.; Lee, C. Low cost exoskeleton manipulator using bidirectional triboelectric sensors enhanced multiple degree of freedom sensory system. *Nat. Commun.* **2021**, *12*, 2692.

[27] Pu, X.; Liu, M. M.; Chen, X. Y.; Sun, J. M.; Du, C. H.; Zhang, Y.; Zhai, J. Y.; Hu, W. G.; Wang, Z. L. Ultrastretchable, transparent triboelectric nanogenerator as electronic skin for biomechanical energy harvesting and tactile sensing. *Sci. Adv.* **2017**, *3*, e1700015.

[28] Wu, H. X.; Su, Z. M.; Shi, M. Y.; Miao, L. M.; Song, Y.; Chen, H. T.; Han, M. D.; Zhang, H. X. Self-powered noncontact electronic skin for motion sensing. *Adv. Funct. Mater.* **2018**, *28*, 1704641.

[29] Shen, S.; Yi, J.; Sun, Z. D.; Guo, Z. H.; He, T. Y.; Ma, L. Y.; Li, H. M.; Fu, J. J.; Lee, C.; Wang, Z. L. Human machine interface with wearable electronics using biodegradable triboelectric films for calligraphy practice and correction. *Nano-Micro Lett.* **2022**, *14*, 225.

[30] Zhu, M. L.; Sun, Z. D.; Zhang, Z. X.; Shi, Q. F.; He, T. Y.; Liu, H. C.; Chen, T.; Lee, C. Haptic-feedback smart glove as a creative human–machine interface (HMI) for virtual/augmented reality applications. *Sci. Adv.* **2020**, *6*, eaaz8693.

[31] Wang, H. Y.; Fu, J. J.; Wang, J. Q.; Su, L.; Zi, Y. L. Tribophotonics: An emerging self-powered wireless solution toward smart city. *Nano Energy* **2022**, *97*, 107196.

[32] Jiang, C. M.; Li, X. J.; Ying, Y. B.; Ping, J. F. A multifunctional TENG yarn integrated into agrotextile for building intelligent agriculture. *Nano Energy* **2020**, *74*, 104863.

[33] Li, X. J.; Luo, J. J.; Han, K.; Shi, X.; Ren, Z. W.; Xi, Y.; Ying, Y. B.; Ping, J. F.; Wang, Z. L. Stimulation of ambient energy generated electric field on crop plant growth. *Nat. Food* **2022**, *3*, 133–142.

[34] Dong, K.; Peng, X.; An, J.; Wang, A. C.; Luo, J. J.; Sun, B. Z.; Wang, J.; Wang, Z. L. Shape adaptable and highly resilient 3D braided triboelectric nanogenerators as e-textiles for power and sensing. *Nat. Commun.* **2020**, *11*, 2868.

[35] Wang, Z. L. From contact electrification to triboelectric nanogenerators. *Rep. Prog. Phys.* **2021**, *84*, 096502.

[36] Wu, H.; Wang, S.; Wang, Z. K.; Zi, Y. L. Achieving ultrahigh instantaneous power density of 10 MW/m^2 by leveraging the opposite-charge-enhanced transistor-like triboelectric nanogenerator (OCT-TENG). *Nat. Commun.* **2021**, *12*, 5470.

[37] He, W. C.; Liu, W. L.; Fu, S. K.; Wu, H. Y.; Shan, C. C.; Wang, Z.; Xi, Y.; Wang, X.; Guo, H. Y.; Liu, H. et al. Ultrahigh performance triboelectric nanogenerator enabled by charge transmission in interfacial lubrication and potential decentralization design. *Research* **2022**, *2022*, 9812865.

[38] He, W. C.; Shan, C. C.; Fu, S. K.; Wu, H. Y.; Wang, J.; Mu, Q. J.; Li, G.; Hu, C. G. Large harvested energy by self-excited liquid suspension triboelectric nanogenerator with optimized charge transportation behavior. *Adv. Mater.* **2023**, *35*, 2209657.

[39] Li, A. Y.; Zi, Y. L.; Guo, H. Y.; Wang, Z. L.; Fernández, F. M. Triboelectric nanogenerators for sensitive nano-coulomb molecular mass spectrometry. *Nat. Nanotechnol.* **2017**, *12*, 481–487.

[40] Cheng, J.; Ding, W. B.; Zi, Y. L.; Lu, Y. J.; Ji, L. H.; Liu, F.; Wu, C. S.; Wang, Z. L. Triboelectric microplasma powered by mechanical stimuli. *Nat. Commun.* **2018**, *9*, 3733.

[41] Guo, H. Y.; Chen, J.; Wang, L. F.; Wang, A. C.; Li, Y. F.; An, C. H.; He, J. H.; Hu, C. G.; Hsiao, V. K. S.; Wang, Z. L. A highly efficient triboelectric negative air ion generator. *Nat. Sustain.* **2021**, *4*, 147–153.

[42] Xu, W. H.; Jin, Y. K.; Li, W. B.; Song, Y. X.; Gao, S. W.; Zhang, B. P.; Wang, L. L.; Cui, M. M.; Yan, X. T.; Wang, Z. K. Triboelectric wetting for continuous droplet transport. *Sci. Adv.* **2022**, *8*, eade2085.

[43] Sun, J. F.; Zhang, L. J.; Zhou, Y. H.; Li, Z. J.; Libanori, A.; Tang, Q.; Huang, Y. Z.; Hu, C. G.; Guo, H. Y.; Peng, Y. et al. Highly efficient liquid droplet manipulation via human-motion-induced direct charge injection. *Mater. Today* **2022**, *58*, 41–47.

[44] Fan, F. R.; Lin, L.; Zhu, G.; Wu, W. Z.; Zhang, R.; Wang, Z. L. Transparent triboelectric nanogenerators and self-powered pressure sensors based on micropatterned plastic films. *Nano Lett.* **2012**, *12*, 3109–3114.

[45] Wang, S. H.; Lin, L.; Wang, Z. L. Nanoscale triboelectric-effect-enabled energy conversion for sustainably powering portable electronics. *Nano Lett.* **2012**, *12*, 6339–6346.

[46] Xu, L.; Bu, T. Z.; Yang, X. D.; Zhang, C.; Wang, Z. L. Ultrahigh charge density realized by charge pumping at ambient conditions for triboelectric nanogenerators. *Nano Energy* **2018**, *49*, 625–633.

[47] Li, S. Y.; Nie, J. H.; Shi, Y. X.; Tao, X. L.; Wang, F.; Tian, J. W.; Lin, S. Q.; Chen, X. Y.; Wang, Z. L. Contributions of different functional groups to contact electrification of polymers. *Adv. Mater.* **2020**, *32*, 2001307.

[48] Cheng, L.; Xu, Q.; Zheng, Y. B.; Jia, X. F.; Qin, Y. A self-improving triboelectric nanogenerator with improved charge density and increased charge accumulation speed. *Nat. Commun.* **2018**, *9*, 3773.

[49] Wang, J.; Li, S. M.; Yi, F.; Zi, Y. L.; Lin, J.; Wang, X. F.; Xu, Y. L.; Wang, Z. L. Sustainably powering wearable electronics solely by biomechanical energy. *Nat. Commun.* **2016**, *7*, 12744.

[50] Liu, W. L.; Wang, Z.; Wang, G.; Liu, G. L.; Chen, J.; Pu, X. J.; Xi, Y.; Wang, X.; Guo, H. Y.; Hu, C. G. et al. Integrated charge excitation triboelectric nanogenerator. *Nat. Commun.* **2019**, *10*, 1426.

[51] Wu, H. Y.; He, W. C.; Shan, C. C.; Wang, Z.; Fu, S. K.; Tang, Q.; Guo, H. Y.; Du, Y.; Liu, W. L.; Hu, C. G. Achieving remarkable charge density via self-polarization of polar high-k material in a charge-excitation triboelectric nanogenerator. *Adv. Mater.* **2022**, *34*, 2109918.

[52] Wang, S. H.; Xie, Y. N.; Niu, S. M.; Lin, L.; Wang, Z. L. Freestanding triboelectric-layer-based nanogenerators for harvesting energy from a moving object or human motion in contact and non-contact modes. *Adv. Mater.* **2014**, *26*, 2818–2824.

[53] Yin, X.; Liu, D.; Zhou, L. L.; Li, X. Y.; Zhang, C. L.; Cheng, P.; Guo, H. Y.; Song, W. X.; Wang, J.; Wang, Z. L. Structure and dimension effects on the performance of layered triboelectric nanogenerators in contact–separation mode. *ACS Nano* **2019**, *13*, 698–705.

[54] Lei, R.; Shi, Y. X.; Ding, Y. F.; Nie, J. H.; Li, S. Y.; Wang, F.; Zhai, H.; Chen, X. Y.; Wang, Z. L. Sustainable high-voltage source based on triboelectric nanogenerator with a charge accumulation strategy. *Energy Environ. Sci.* **2020**, *13*, 2178–2190.

[55] He, W. C.; Liu, W. L.; Chen, J.; Wang, Z.; Liu, Y. K.; Pu, X. J.; Yang, H. M.; Tang, Q.; Yang, H. K.; Guo, H. Y. et al. Boosting output performance of sliding mode triboelectric nanogenerator by charge space-accumulation effect. *Nat. Commun.* **2020**, *11*, 4277.

[56] Zhou, L. L.; Liu, D.; Zhao, Z. H.; Li, S. X.; Liu, Y. B.; Liu, L.;

Gao, Y. K.; Wang, Z. L.; Wang, J. Simultaneously enhancing power density and durability of sliding-mode triboelectric nanogenerator via interface liquid lubrication. *Adv. Energy Mater.* **2020**, *10*, 2002920.
[57] Wang, Z. L.; Wang, A. C. On the origin of contact-electrification. *Mater. Today* **2019**, *30*, 34–51.
[58] Shaw, P. E. The electrical charges from like solids. *Nature* **1926**, *118*, 659–660.
[59] Li, S. M.; Zhou, Y. S.; Zi, Y. L.; Zhang, G.; Wang, Z. L. Excluding contact electrification in surface potential measurement using kelvin probe force microscopy. *ACS Nano* **2016**, *10*, 2528–2535.
[60] Zhou, Y. S.; Liu, Y.; Zhu, G.; Lin, Z. H.; Pan, C. F.; Jing, Q. S.; Wang, Z. L. *In situ* quantitative study of nanoscale triboelectrification and patterning. *Nano Lett.* **2013**, *13*, 2771–2776.
[61] Zhou, Y. S.; Li, S. M.; Niu, S. M.; Wang, Z. L. Effect of contact- and sliding-mode electrification on nanoscale charge transfer for energy harvesting. *Nano Res.* **2016**, *9*, 3705–3713.
[62] Zhou, Y. S.; Wang, S. H.; Yang, Y.; Zhu, G.; Niu, S. M.; Lin, Z. H.; Liu, Y.; Wang, Z. L. Manipulating nanoscale contact electrification by an applied electric field. *Nano Lett.* **2014**, *14*, 1567–1572.
[63] Lin, S. Q.; Xu, C.; Xu, L.; Wang, Z. L. The overlapped electron-cloud model for electron transfer in contact electrification. *Adv. Funct. Mater.* **2020**, *30*, 1909724.
[64] Cao, Z. Y.; Wu, Z. B.; Ding, R.; Wang, S. W.; Chu, Y.; Xu, J. N.; Teng, J. C.; Ye, X. Y. A compact triboelectric nanogenerator with ultrahigh output energy density of 177.8 $J \cdot m^{-3}$ via retarding air breakdown. *Nano Energy* **2022**, *93*, 106891.
[65] Zhang, J. Y.; Li, S. X.; Zhao, Z. H.; Gao, Y. K.; Liu, D.; Wang, J.; Wang, Z. L. Highly sensitive three-dimensional scanning triboelectric sensor for digital twin applications. *Nano Energy* **2022**, *97*, 107198.
[66] Yuan, W.; Zhang, C. G.; Zhang, B. F.; Wei, X. L.; Yang, O.; Liu, Y. B.; He, L. X.; Cui, S. N.; Wang, J.; Wang, Z. L. Wearable, breathable, and waterproof triboelectric nanogenerators for harvesting human motion and raindrop energy. *Adv. Mater. Technol.* **2022**, *7*, 2101139.
[67] Sun, J. F.; Zhang, L. J.; Li, Z. J.; Tang, Q.; Chen, J.; Huang, Y. Z.; Hu, C. G.; Guo, H. Y.; Peng, Y.; Wang, Z. L. A mobile and self-powered micro-flow pump based on triboelectricity driven electroosmosis. *Adv. Mater.* **2021**, *33*, 2102765.
[68] Peng, X.; Dong, K.; Ye, C. Y.; Jiang, Y.; Zhai, S. Y.; Cheng, R. W.; Liu, D.; Gao, X. P.; Wang, J.; Wang, Z. L. A breathable, biodegradable, antibacterial, and self-powered electronic skin based on all-nanofiber triboelectric nanogenerators. *Sci. Adv.* **2020**, *6*, eaba9624.
[69] Qin, K.; Chen, C.; Pu, X. J.; Tang, Q.; He, W. C.; Liu, Y. K.; Zeng, Q. X.; Liu, G. L.; Guo, H. Y.; Hu, C. G. Magnetic array assisted triboelectric nanogenerator sensor for real-time gesture interaction. *Nano-Micro Lett.* **2021**, *13*, 51.
[70] Shi, Q. F.; Wu, H.; Wang, H.; Wu, H. X.; Lee, C. Self-powered gyroscope ball using a triboelectric mechanism. *Adv. Energy Mater.* **2017**, *7*, 1701300.
[71] Zeng, Y. M.; Luo, Y.; Lu, Y. R.; Cao, X. Self-powered rain droplet sensor based on a liquid–solid triboelectric nanogenerator. *Nano Energy* **2022**, *98*, 107316.
[72] He, L. X.; Zhang, C. G.; Zhang, B. F.; Yang, O.; Yuan, W.; Zhou, L. L.; Zhao, Z. H.; Wu, Z. Y.; Wang, J.; Wang, Z. L. A dual-mode triboelectric nanogenerator for wind energy harvesting and self-powered wind speed monitoring. *ACS Nano* **2022**, *16*, 6244–6254.
[73] Wang, Z. M.; An, J.; Nie, J. H.; Luo, J. J.; Shao, J. J.; Jiang, T.; Chen, B. D.; Tang, W.; Wang, Z. L. A self-powered angle sensor at nanoradian-resolution for robotic arms and personalized medicare. *Adv. Mater.* **2020**, *32*, 2001466.
[74] Shao, J. J.; Liu, D.; Willatzen, M.; Wang, Z. L. Three-dimensional modeling of alternating current triboelectric nanogenerator in the linear sliding mode. *Appl. Phys. Rev.* **2020**, *7*, 011405.
[75] Dharmasena, R. D. I. G.; Jayawardena, K. D. G. I.; Mills, C. A.; Deane, J. H. B.; Anguita, J. V.; Dorey, R. A.; Silva, S. R. P. Triboelectric nanogenerators: Providing a fundamental framework. *Energy Environ. Sci.* **2017**, *10*, 1801–1811.
[76] Wang, Z. L. On the first principle theory of nanogenerators from Maxwell's equations. *Nano Energy* **2020**, *68*, 104272.
[77] Zi, Y. L.; Niu, S. M.; Wang, J.; Wen, Z.; Tang, W.; Wang, Z. L. Standards and figure-of-merits for quantifying the performance of triboelectric nanogenerators. *Nat. Commun.* **2015**, *6*, 8376.
[78] Xia, X.; Fu, J. J.; Zi, Y. L. A universal standardized method for output capability assessment of nanogenerators. *Nat. Commun.* **2019**, *10*, 4428.
[79] Wang, J.; Wu, C. S.; Dai, Y. J.; Zhao, Z. H.; Wang, A.; Zhang, T. J.; Wang, Z. L. Achieving ultrahigh triboelectric charge density for efficient energy harvesting. *Nat. Commun.* **2017**, *8*, 88.
[80] Wang, S. H.; Xie, Y. N.; Niu, S. M.; Lin, L.; Liu, C.; Zhou, Y. S.; Wang, Z. L. Maximum surface charge density for triboelectric nanogenerators achieved by ionized-air injection: Methodology and theoretical understanding. *Adv. Mater.* **2014**, *26*, 6720–6728.
[81] Liu, D.; Zhou, L. L.; Cui, S. N.; Gao, Y. K.; Li, S. X.; Zhao, Z. H.; Yi, Z. Y.; Zou, H. Y.; Fan, Y. J.; Wang, J. et al. Standardized measurement of dielectric materials' intrinsic triboelectric charge density through the suppression of air breakdown. *Nat. Commun.* **2022**, *13*, 6019.
[82] Zi, Y. L.; Wu, C. S.; Ding, W. B.; Wang, Z. L. Maximized effective energy output of contact–separation-triggered triboelectric nanogenerators as limited by air breakdown. *Adv. Funct. Mater.* **2017**, *27*, 1700049.
[83] Zhang, C. L.; Zhou, L. L.; Cheng, P.; Yin, X.; Liu, D.; Li, X. Y.; Guo, H. Y.; Wang, Z. L.; Wang, J. Surface charge density of triboelectric nanogenerators: Theoretical boundary and optimization methodology. *Appl. Mater. Today* **2020**, *18*, 100496.
[84] Fu, J. J.; Xia, X.; Xu, G. Q.; Li, X. Y.; Zi, Y. L. On the maximal output energy density of nanogenerators. *ACS Nano* **2019**, *13*, 13257–13263.
[85] Zou, H. Y.; Zhang, Y.; Guo, L. T.; Wang, P. H.; He, X.; Dai, G. Z.; Zheng, H. W.; Chen, C. Y.; Wang, A. C.; Xu, C. et al. Quantifying the triboelectric series. *Nat. Commun.* **2019**, *10*, 1427.
[86] Yang, W. X.; Wang, X. L.; Li, H. Q.; Wu, J.; Hu, Y. Q.; Li, Z. H.; Liu, H. Fundamental research on the effective contact area of micro-/nano-textured surface in triboelectric nanogenerator. *Nano Energy* **2019**, *57*, 41–47.
[87] Verners, O.; Lapčinskis, L.; Ģermane, L.; Kasikov, A.; Timusk, M.; Pudzs, K.; Ellis, A. V.; Sherrell, P. C.; Šutka, A. Smooth polymers charge negatively: Controlling contact electrification polarity in polymers. *Nano Energy* **2022**, *104*, 107914.
[88] Wang, S. H.; Zi, Y. L.; Zhou, Y. S.; Li, S. M.; Fan, F. R.; Lin, L.; Wang, Z. L. Molecular surface functionalization to enhance the power output of triboelectric nanogenerators. *J. Mater. Chem. A* **2016**, *4*, 3728–3734.
[89] Shin, S. H.; Kwon, Y. H.; Kim, Y. H.; Jung, J. Y.; Lee, M. H.; Nah, J. Triboelectric charging sequence induced by surface functionalization as a method to fabricate high performance triboelectric generators. *ACS Nano* **2015**, *9*, 4621–4627.
[90] Song, G.; Kim, Y.; Yu, S.; Kim, M. O.; Park, S. H.; Cho, S. M.; Velusamy, D. B.; Cho, S. H.; Kim, K. L.; Kim, J. et al. Molecularly engineered surface triboelectric nanogenerator by self-assembled monolayers (METS). *Chem. Mater.* **2015**, *27*, 4749–4755.
[91] Yu, B.; Yu, H.; Huang, T.; Wang, H. Z.; Zhu, M. F. A biomimetic nanofiber-based triboelectric nanogenerator with an ultrahigh transfer charge density. *Nano Energy* **2018**, *48*, 464–470.
[92] Chun, J. S.; Ye, B. U.; Lee, J. W.; Choi, D.; Kang, C. Y.; Kim, S. W.; Wang, Z. L.; Baik, J. M. Boosted output performance of triboelectric nanogenerator via electric double layer effect. *Nat. Commun.* **2016**, *7*, 12985.
[93] Fu, J. J.; Xu, G. Q.; Li, C. H.; Xia, X.; Guan, D.; Li, J.; Huang, Z. Y.; Zi, Y. L. Achieving ultrahigh output energy density of triboelectric nanogenerators in high-pressure gas environment. *Adv. Sci.* **2020**, *7*, 2001757.
[94] Lin, S. Q.; Xu, L.; Xu, C.; Chen, X. Y.; Wang, A. C.; Zhang, B. B.; Lin, P.; Yang, Y.; Zhao, H. B.; Wang, Z. L. Electron transfer in nanoscale contact electrification: Effect of temperature in the metal-dielectric case. *Adv. Mater.* **2019**, *31*, 1808197.
[95] Xu, C.; Zi, Y. L.; Wang, A. C.; Zou, H. Y.; Dai, Y. J.; He, X.; Wang, P. H.; Wang, Y. C.; Feng, P. Z.; Li, D. W. et al. On the

electron-transfer mechanism in the contact-electrification effect. *Adv. Mater.* **2018**, *30*, 1706790.
[96] Cheng, B. L.; Xu, Q.; Ding, Y. Q.; Bai, S.; Jia, X. F.; Yu, Y. D. C.; Wen, J.; Qin, Y. High performance temperature difference triboelectric nanogenerator. *Nat. Commun.* **2021**, *12*, 4782.
[97] Wang, K.; Qiu, Z. R.; Wang, J. X.; Liu, Y.; Chen, R.; An, H. Q.; Park, J. H.; Suk, C. H.; Wu, C. X.; Lin, J. T. et al. Effect of relative humidity on the enhancement of the triboelectrification efficiency utilizing water bridges between triboelectric materials. *Nano Energy* **2022**, *93*, 106880.
[98] Liu, L.; Zhou, L. L.; Zhang, C. G.; Zhao, Z. H.; Li, S. X.; Li, X. Y.; Yin, X.; Wang, J.; Wang, Z. L. A high humidity-resistive triboelectric nanogenerator via coupling of dielectric material selection and surface-charge engineering. *J. Mater. Chem. A* **2021**, *9*, 21357–21365.
[99] Wu, J.; Xi, Y. H.; Shi, Y. J. Toward wear-resistive, highly durable, and high performance triboelectric nanogenerator through interface liquid lubrication. *Nano Energy* **2020**, *72*, 104659.
[100] Liu, Y. K.; Liu, W. L.; Wang, Z.; He, W. C.; Tang, Q.; Xi, Y.; Wang, X.; Guo, H. Y.; Hu, C. G. Quantifying contact status and the air-breakdown model of charge-excitation triboelectric nanogenerators to maximize charge density. *Nat. Commun.* **2020**, *11*, 1599.
[101] Li, Y. H.; Zhao, Z. H.; Liu, L.; Zhou, L. L.; Liu, D.; Li, S. X.; Chen, S. Y.; Dai, Y. J.; Wang, J.; Wang, Z. L. Improved output performance of triboelectric nanogenerator by fast accumulation process of surface charges. *Adv. Energy Mater.* **2021**, *11*, 2100050.
[102] Zhou, L. L.; Gao, Y. K.; Liu, D.; Liu, L.; Zhao, Z. H.; Li, S. X.; Yuan, W.; Cui, S. N.; Wang, Z. L.; Wang, J. Achieving ultrarobust and humidity-resistant triboelectric nanogenerator by dual-capacitor enhancement system. *Adv. Energy Mater.*, in press, https://doi.org/10.1002/aenm.202101958.
[103] Lei, R.; Li, S. Y.; Shi, Y. X.; Yang, P.; Tao, X. L.; Zhai, H.; Wang, Z. L.; Chen, X. Y. Largely enhanced output of the non-contact mode triboelectric nanogenerator via a charge excitation based on a high insulation strategy. *Adv. Energy Mater.* **2022**, *12*, 2201708.
[104] Liu, L.; Zhao, Z. H.; Li, Y. H.; Li, X. Y.; Liu, D.; Li, S. X.; Gao, Y. K.; Zhou, L. L.; Wang, J.; Wang, Z. L. Achieving ultrahigh effective surface charge density of direct-current triboelectric nanogenerator in high humidity. *Small* **2022**, *18*, 2201402.
[105] Dai, K. R.; Liu, D.; Yin, Y. J.; Wang, X. F.; Wang, J.; You, Z.; Zhang, H.; Wang, Z. L. Transient physical modeling and comprehensive optimal design of air-breakdown direct-current triboelectric nanogenerators. *Nano Energy* **2022**, *92*, 106742.
[106] Zhao, Z. H.; Dai, Y. J.; Liu, D.; Zhou, L. L.; Li, S. X.; Wang, Z. L.; Wang, J. Rationally patterned electrode of direct-current triboelectric nanogenerators for ultrahigh effective surface charge density. *Nat. Commun.* **2020**, *11*, 6186.
[107] Liu, D.; Zhou, L. L.; Li, S. X.; Zhao, Z. H.; Yin, X.; Yi, Z. Y.; Zhang, C. L.; Li, X. Y.; Wang, J.; Wang, Z. L. Hugely enhanced output power of direct-current triboelectric nanogenerators by using electrostatic breakdown effect. *Adv. Mater. Technol.* **2020**, *5*, 2000289.
[108] Liu, D.; Yin, X.; Guo, H. Y.; Zhou, L. L.; Li, X. Y.; Zhang, C. L.; Wang, J.; Wang, Z. L. A constant current triboelectric nanogenerator arising from electrostatic breakdown. *Sci. Adv.* **2019**, *5*, eaav6437.
[109] Zhao, Z. H.; Zhou, L. L.; Li, S. X.; Liu, D.; Li, Y. H.; Gao, Y. K.; Liu, Y. B.; Dai, Y. J.; Wang, J.; Wang, Z. L. Selection rules of triboelectric materials for direct-current triboelectric nanogenerator. *Nat. Commun.* **2021**, *12*, 4686.
[110] Gao, Y. K.; Liu, D.; Zhou, L. L.; Li, S. X.; Zhao, Z. H.; Yin, X.; Chen, S. Y.; Wang, Z. L.; Wang, J. A robust rolling-mode direct-current triboelectric nanogenerator arising from electrostatic breakdown effect. *Nano Energy* **2021**, *85*, 106014.
[111] Chen, S. Y.; Liu, D.; Zhou, L. L.; Li, S. X.; Zhao, Z. H.; Cui, S. N.; Gao, Y. K.; Li, Y. H.; Wang, Z. L.; Wang, J. Improved output performance of direct-current triboelectric nanogenerator through field enhancing breakdown effect. *Adv. Mater. Technol.* **2021**, *6*, 2100195.
[112] Cui, S. N.; Zhou, L. L.; Liu, D.; Li, S. X.; Liu, L.; Chen, S. Y.; Zhao, Z. H.; Yuan, W.; Wang, Z. L.; Wang, J. Improving performance of triboelectric nanogenerators by dielectric enhancement effect. *Matter* **2022**, *5*, 180–193.
[113] Zhou, L. L.; Liu, D.; Li, S. X.; Zhao, Z. H.; Zhang, C. L.; Yin, X.; Liu, L.; Cui, S. N.; Wang, Z. L.; Wang, J. Rationally designed dual-mode triboelectric nanogenerator for harvesting mechanical energy by both electrostatic induction and dielectric breakdown effects. *Adv. Energy Mater.* **2020**, *10*, 2000965.
[114] Wang, Z. Z.; Zhang, Z.; Chen, Y. K.; Gong, L. K.; Dong, S. C.; Zhou, H.; Lin, Y.; Lv, Y.; Liu, G. X.; Zhang, C. Achieving an ultrahigh direct-current voltage of 130 V by semiconductor heterojunction power generation based on the tribovoltaic effect. *Energy Environ. Sci.* **2022**, *15*, 2366–2373.
[115] Zhang, Z.; Wang, Z. Z.; Chen, Y. K.; Feng, Y.; Dong, S. C.; Zhou, H.; Wang, Z. L.; Zhang, C. Semiconductor contact-electrification-dominated tribovoltaic effect for ultrahigh power generation. *Adv. Mater.* **2022**, *34*, 2200146.
[116] Qiao, W. Y.; Zhao, Z. H.; Zhou, L. L.; Liu, D.; Li, S. X.; Yang, P. Y.; Li, X. Y.; Liu, J. Q.; Wang, J.; Wang, Z. L. Simultaneously enhancing direct-current density and lifetime of tribovotaic nanogenerator via interface lubrication. *Adv. Funct. Mater.* **2022**, *32*, 2208544.
[117] Meng, J.; Pan, C. X.; Li, L. W.; Guo, Z. H.; Xu, F.; Jia, L. Y.; Wang, Z. L.; Pu, X. Durable flexible direct current generation through the tribovoltaic effect in contact–separation mode. *Energy Environ. Sci.* **2022**, *15*, 5159–5167.
[118] Meng, J.; Guo, Z. H.; Pan, C. X.; Wang, L. Y.; Chang, C. Y.; Li, L. W.; Pu, X.; Wang, Z. L. Flexible textile direct-current generator based on the tribovoltaic effect at dynamic metal–semiconducting polymer interfaces. *ACS Energy Lett.* **2021**, *6*, 2442–2450.
[119] Wang, Z.; Liu, W. L.; Hu, J. L.; He, W. C.; Yang, H. K.; Ling, C.; Xi, Y.; Wang, X.; Liu, A. P.; Hu, C. G. Two voltages in contact–separation triboelectric nanogenerator: From asymmetry to symmetry for maximum output. *Nano Energy* **2020**, *69*, 104452.
[120] Xu, L.; Wu, H.; Yao, G.; Chen, L. B.; Yang, X. D.; Chen, B. D.; Huang, X.; Zhong, W.; Chen, X. Y.; Yin, Z. P. et al. Giant voltage enhancement via triboelectric charge supplement channel for self-powered electroadhesion. *ACS Nano* **2018**, *12*, 10262–10271.
[121] Wang, Z.; Tang, Q.; Shan, C. C.; Du, Y.; He, W. C.; Fu, S. K.; Li, G.; Liu, A. P.; Liu, W. L.; Hu, C. G. Giant performance improvement of triboelectric nanogenerator systems achieved by matched inductor design. *Energy Environ. Sci.* **2021**, *14*, 6627–6637.
[122] Wang, Z.; Liu, W. L.; He, W. C.; Guo, H. Y.; Long, L.; Xi, Y.; Wang, X.; Liu, A. P.; Hu, C. G. Ultrahigh electricity generation from low-frequency mechanical energy by efficient energy management. *Joule* **2021**, *5*, 441–455.
[123] Dai, K. R.; Wang, X. F.; Niu, S. M.; Yi, F.; Yin, Y. J.; Chen, L.; Zhang, Y.; You, Z. Simulation and structure optimization of triboelectric nanogenerators considering the effects of parasitic capacitance. *Nano Res.* **2017**, *10*, 157–171.
[124] Yang, Z.; Yang, Y. Y.; Wang, H.; Liu, F.; Lu, Y. J.; Ji, L. H.; Wang, Z. L.; Cheng, J. Charge pumping for sliding-mode triboelectric nanogenerator with voltage stabilization and boosted current. *Adv. Energy Mater.* **2021**, *11*, 2101147.
[125] Bai, Y.; Xu, L.; Lin, S. Q.; Luo, J. J.; Qin, H. F.; Han, K.; Wang, Z. L. Charge pumping strategy for rotation and sliding type triboelectric nanogenerators. *Adv. Energy Mater.* **2020**, *10*, 2000605.
[126] Cheng, X. L.; Miao, L. M.; Song, Y.; Su, Z. M.; Chen, H. T.; Chen, X. X.; Zhang, J. X.; Zhang, H. X. High efficiency power management and charge boosting strategy for a triboelectric nanogenerator. *Nano Energy* **2017**, *38*, 438–446.
[127] Xu, S. X.; Zhang, L.; Ding, W. B.; Guo, H. Y.; Wang, X. H.; Wang, Z. L. Self-doubled-rectification of triboelectric nanogenerator. *Nano Energy* **2019**, *66*, 104165.
[128] Peng, J.; Kang, S. D.; Snyder, G. J. Optimization principles and the figure of merit for triboelectric generators. *Sci. Adv.* **2017**, *3*, eaap8576.